

IMPACT OF MACROBEND LOSS ON THE BANDWIDTH OF
STANDARD AND BEND-OPTIMIZED MULTIMODE FIBERS

by
Ying Li

A Dissertation Submitted to the Faculty of the
COLLEGE OF OPTICAL SCIENCES
In Partial Fulfillment of the Requirements
For the Degree of
DOCTOR OF PHILOSOPHY
In the Graduate College
THE UNIVERSITY OF ARIZONA

2009

THE UNIVERSITY OF ARIZONA
GRADUATE COLLEGE

As members of the Dissertation Committee, we certify that we have read the dissertation prepared by Ying Li

entitled Impact of Macrobend Loss on the Bandwidth of Standard and Bend-Optimized Multimode Fibers

and recommend that it be accepted as fulfilling the dissertation requirement for the Degree of Doctor of Philosophy

_____ Date: April 30, 2009
Franko Kueppers

_____ Date: April 30, 2009
Eustace Dereniak

_____ Date: April 30, 2009
Valéria L. da Silva

Final approval and acceptance of this dissertation is contingent upon the candidate's submission of the final copies of the dissertation to the Graduate College. I hereby certify that I have read this dissertation prepared under my direction and recommend that it be accepted as fulfilling the dissertation requirement.

_____ Date: April 30, 2009
Dissertation Director: Franko Kueppers

STATEMENT BY AUTHOR

This dissertation has been submitted in partial fulfillment of requirements for an advanced degree at the University of Arizona and is deposited in the University Library to be made available to borrowers under rules of the Library.

Brief quotations from this dissertation are allowable without special permission, provided that accurate acknowledgment of source is made. Requests for permission for extended quotation from or reproduction of this manuscript in whole or in part may be granted by the head of the major department or the Dean of the Graduate College when in his or her judgment the proposed use of the material is in the interests of scholarship. In all other instances, however, permission must be obtained from the author.

Ying Li

ACKNOWLEDGEMENTS

First of all, I would like to thank my academic advisor Dr. Franko Küppers. I am grateful to him for supporting me and providing me continued opportunity to work on my Ph.D. dissertation. His unconditional support has encouraged me to accomplish this mission. I am also deeply grateful to Dr. Eustace L. Dereniak for his enthusiastic support and advocacy of my work, and for serving on my dissertation defense committee. I am very fortunate to have had him as my mentor since I joined the College of Optical Sciences. Many, many thanks go to the staff in the academic office, especially in the last couple years: Gail Varin, Barbara Martinez, Dr. Shoemaker and Dr. Carl Maes. Without their support, I just cannot image how I would have completed this work off campus in Corning, New York.

I deeply appreciate the support and friendship of my colleagues at Corning Incorporated. In particular, I would like to thank Dr. Valeria L. da Silva, Dr. Scott R. Bickham, and Dr. John S. Abbott for their guidance in my research work and their willingness to share knowledge. A special thank you to Dr. Valeria L. da Silva for serving as a committee member as well. I would like to thank Tony Artuso, Steve C. Garner, and Kevin Bennett for giving me access to their lab and for their generous help and support during the experiments. Also, direct support from the leadership in Corning Specialty Materials Development and Corning Optical Fiber Development including Dr. Ulrich Neukirch, Dr. Xavier Lafosse, and Dr. Aleksandra Boskovic, made it possible for me to complete the dissertation while working at Corning. I am grateful to my coach at Corning Incorporated, Dr. Polly Chu, whose wisdom left a trace in this dissertation path.

I am greatly obliged to my friends in Corning and in Tucson: Aliya Kazmi, Josh Ding, Victoria Chang, Rei Chang, Wayne Liu, Tom Cai, Bill Rosch, Steve Molson, Brian Devaul, Robin Force, Christie Mendola, Ivan Cornejo, Sam Zoubi, Sadashiva Pai, Paul Cai, Yuan Qu, and Freda Phifer... so many people who came across and offered their help and provided me with encouragement during this long journey. I just cannot list them all. Special thanks to Dr. Kit-Iu Cheong who shared her dissertation experience with me and gave me the confidence I needed to complete my dissertation. I would like to thank Dr. Johannes Moll for reviewing my manuscript and providing valuable feedback. And Deepti Mudaliar, all your prayers finally got answered!

Most importantly, I would like to thank my family for their unconditional faith/belief in me. I am especially thankful to my dear parents, who gave me this wonderful life to appreciate.

*To my dear mother, Yujie,
and in the memory of my dear father, Yonghe...
Their endless love is my inspiration.*

TABLE OF CONTENTS

LIST OF FIGURES	8
ABSTRACT	11
CHAPTER 1. INTRODUCTION	13
1.1. Ethernet Network Development	13
1.2. Scope of Study	15
CHAPTER 2. 10 GIGABIT ETHERNET FIBER-OPTICS	17
2.1. Optical Fiber Basics	17
2.2. Single-mode Fiber and Multi-mode Fiber	19
2.2.1. Single-mode Fiber	19
2.2.2. Multi-mode Fiber	20
2.3. Optical Transmitters	22
CHAPTER 3. MODAL DISPERSION IN MULTIMODE FIBER	24
3.1. Modes in Optical Fibers	24
3.2. Attenuation and Dispersion	31
3.2.1. Attenuation	31
3.2.2. Dispersion	31
3.2.3. Effects of Dispersion and Attenuation	32
3.3. Intermodal Dispersion Measurement	33
3.3.1. MMF Mode Groups	33
3.3.2. Differential Mode Delay Measurement	33
CHAPTER 4. MULTIMODE FIBER LAUNCH CONDITIONS	36
4.1. Overfilled Launch (OFL) and Laser Source Launch	36
4.2. Encircled Flux Launch (EFL)	37
4.3. MMF Macrobend Loss with OFL and EFL	40
4.3.1. Experimental Setup	42
4.3.2. Results and Findings	45
CHAPTER 5. IMPACT OF MACROBEND LOSS ON BANDWIDTH	51
5.1. Bandwidth	51
5.2. DMD Traces Change with Macrobending	52
5.3. Impact of Macrobend Loss	55
5.3.1. Experimental Setup	55
5.3.2. Results and Findings	58

TABLE OF CONTENTS—*Continued*

CHAPTER 6. IMPACT OF MACROBENDING ON OPTICAL LINK PERFORMANCE	60
6.1. Optical Fiber Data Link	60
6.2. 10 Gigabit Ethernet Link Model	61
6.3. Results and Findings	65
CHAPTER 7. CONCLUSIONS AND FUTURE WORK	70
7.1. Conclusions	70
7.2. Future Work	71
REFERENCES	73

LIST OF FIGURES

FIGURE 1.1. Premises network links	14
FIGURE 2.1. Schematic of a fiber structure	17
FIGURE 2.2. Refraction, critical angle and total internal reflection at a material boundary	18
FIGURE 2.3. The propagation mechanism in an ideal step-index optical fiber	19
FIGURE 2.4. Single-mode fiber	20
FIGURE 2.5. Step-index multimode fiber	21
FIGURE 2.6. Comparison of types of optical fiber designs.(a) single-mode fiber, both stepped-index and graded-index are possible, (b) stepped-index MMF, (c) graded- index MMF.	22
FIGURE 3.1. Matlab simulation of intensity distribution of first 12 LP modes in a step-index fiber	29
FIGURE 3.2. Normalized propagation constant b as a function of V	30
FIGURE 3.3. Effects of dispersion and attenuation	32
FIGURE 3.4. Differential modal delay measurement scan	34
FIGURE 3.5. DMD measurement result of standard MMF1	34
FIGURE 3.6. DMD measurement result of standard MMF2	35
FIGURE 4.1. Launch conditions for commonly used fiber-optic light sources .	36
FIGURE 4.2. VCSEL near-field power distribution pattern	38
FIGURE 4.3. VCSEL EF boundary conditions specified for 10 GbE	38
FIGURE 4.4. EF Curves for nominal OFL, LPS and Target EF for 50 μm fibers from Tom A. Hanson's report	39
FIGURE 4.5. Mode groups power distribution at near-field of a standard OM3 MMF with OFL and EFL	40
FIGURE 4.6. Macrobend loss occurs where TIR fails, and a portion of the mode field escapes.	41
FIGURE 4.7. PK 2500 fiber analysis system	42
FIGURE 4.8. Fiber holder inserted in cleaver FK 11	43
FIGURE 4.9. Fiber inserted in a SIECOR cleaver	44
FIGURE 4.10. Ericsson fusion splicer	44
FIGURE 4.11. Macrobend loss measurement setup with an OFL	45
FIGURE 4.12. Macrobend loss measurement setup with an EFL	45
FIGURE 4.13. Spectral scan of standard MMF2 OFL bend loss measurement with 1 turn at 7.5 mm bend radius	46
FIGURE 4.14. Measured OFL bend loss at 850 nm with different number of turns at different bend radii. (a) standard MMF1, (b) standard MMF2 .	47

LIST OF FIGURES—*Continued*

FIGURE 4.15. Measured EFL bend loss at 850 nm with different number of turns at different bend radii. (a) standard MMF1, (b) standard MMF2 .	47
FIGURE 4.16. Comparison of standard MMF1 bend loss performance with (a) OFL and (b) EFL	48
FIGURE 4.17. Measured bend loss of bend optimized MMF at 850 nm (a) OFL, (b) EFL	49
FIGURE 4.18. Bend loss of standard MMF1, standard MMF2, and BO MMF at 850 nm with an EFL using a 5 mm radius mandrel	49
FIGURE 5.1. Transfer function	52
FIGURE 5.2. DMD measurement of standard MMF1 at 850nm. (a) no mandrel bend (b) 1 turn at 5 mm radius	52
FIGURE 5.3. Pulse measurement of standard MMF1 at 850nm.	53
FIGURE 5.4. DMD measurement of standard MMF2 at 850nm. (a) no mandrel bend (b) 1 turn at 5 mm radius	54
FIGURE 5.5. Pulse measurement of standard MMF1 at 850nm.	54
FIGURE 5.6. DMD measurement result of BO-MMF	55
FIGURE 5.7. Examples of measured pulse spreading $P_{out}(t)$ of standard MMF1 with an OFL	56
FIGURE 5.8. Examples of measured pulse spreading $P_{in}(t)$ of standard MMF1 with an OFL	56
FIGURE 5.9. Examples of bandwidth f identification of standard MMF1 with an OFL	57
FIGURE 5.10. Bandwidth measurement setup with an OFL	58
FIGURE 5.11. Bandwidth measurement setup with an EFL	58
FIGURE 5.12. Impact of macrobend loss on bandwidth with OFL and EFL for standard MMFs	59
FIGURE 5.13. Impact of macrobending on bandwidth of bend optimized MMF, compared to standard MMFs.	59
FIGURE 6.1. SC and ST connectors	60
FIGURE 6.2. Typical optical fiber link diagram	61
FIGURE 6.3. Optical link power budget	62
FIGURE 6.4. Portion of the IEEE 10GEPBud3_1_16a.xls spreadsheet	64
FIGURE 6.5. An eye diagram shows the presence of ISI	65
FIGURE 6.6. Standard MMF1 with no bend, with an OFL	65
FIGURE 6.7. Standard MMF1 with 1 turn at 7.5 mm bend radius, with an OFL	66
FIGURE 6.8. Standard MMF1 with 10 turn at 5 mm bend radius, with an OFL	66
FIGURE 6.9. BO- MMF with 10 turn at 7.5 mm bend radius, with an OFL	67
FIGURE 6.10. P_{ISI} at 5 mm bend radius with OFL	67
FIGURE 6.11. P_{ISI} at 5 mm bend radius with EFL	68

LIST OF FIGURES—*Continued*

FIGURE 6.12. Link margin at 5 mm bend radius with OFL	68
FIGURE 6.13. Link margin at 5 mm bend radius with EFL	69
FIGURE 7.1. Example of very high bandwidth measurement result	71

ABSTRACT

10 Gigabit Ethernet (GbE) demands faster optical sources to support high modulation rates. At the same time, the allowable margin in the 10 GbE link power budget is decreasing. This means that a 10 GbE system is unable to support as many tight bends, and it is more difficult to avoid the costly downtime that results when the allowable margin is exceeded. The recent introduction of bend-optimized (BO) multimode fiber (MMF) provides a clear solution. 850 nm vertical cavity surface emitting lasers (VCSELs) and MMFs have long been the most cost effective choice for short reach premise applications. As will be shown, the combination of BO-MMF with VCSELs is even more attractive.

Historically, MMF systems operating at low bit rates of 10-100 Mbps used light-emitting diodes (LED) sources, which launch nearly equal power into every fiber mode. This launch is approximated by the overfilled launch (OFL), which is still used to characterize the core diameter and numerical aperture of MMF. Unlike LEDs, VCSELs typically underfill the fiber core and are better represented by an encircled flux launch (EFL). Using OFL to evaluate a VCSEL-based MMF system could therefore produce inaccurate and misleading results. A recent study [1] characterized the macrobend loss of MMF with overfilled and restricted mode offset launch conditions. In this study, the MMFs performance with an EFL is evaluated, which is a more relevant launch condition for laser transmission. The impact of both launch conditions, OFL and EFL, on MMF performance is studied and compared.

Macrobend losses at small bend radii and their impact on the bandwidth for both standard 50/125 μm MMF and a newly introduced BO-MMF are characterized. In addition, the 10 GbE link performance is also evaluated using the IEEE link model P802.3ae3. The simulation results illustrate that both macrobend loss and bandwidth are vital to the overall optical link performance. The 10 GbE link performance of

the standard fiber deteriorates with macrobends, while the bend-optimized fiber is insensitive to the deployment conditions.

Chapter 1

INTRODUCTION

1.1 Ethernet Network Development

Ethernet was originally developed between 1973 and 1975 by the Xerox Corporation at their Palo Alto Research Center in California [2] to operate at a data rate of 3 megabits per second (Mbps) using a carrier sense multiple access collision detect (CSMA/CD) protocol for local area networks (LANs) with infrequent but sporadically heavy traffic requirements. In 1980 there was a joint effort by DEC, Intel, and Xerox to promote Ethernet as a standard, i.e. 10 Mbps Ethernet Version 1.0 specification. Ethernet then became the Institute of Electrical and Electronics Engineers, Inc. (IEEE) standard for connecting personal computers via a LAN in 1985. The original IEEE 802.3 standard was based on the Ethernet Version 1.0 specification. Fast Ethernet enhanced the speed from 10 to 100 Mbps. Gigabit Ethernet (GbE), as the next generation, increased the speed to 1000 Mbps in 1998. Since then, a 10 GbE fiber-based standard was first published in 2002 as IEEE standard 802.3ae-2002. It is the fastest of the Ethernet standards so far with a data rate of 10 gigabits per second (Gbps). Today, Ethernet has evolved into the most widely implemented physical and link layer protocol. It has been estimated that over 70 percent of the worlds networks use the Ethernet protocol.

As shown in Figure 1.1 [3][4], a typical Ethernet premises network consists of four types of links: the backbone, the vertical riser, the horizontal interconnect and the data center. The *backbone* is the main cable that ties different networks in separated buildings on site together. The physical medium connecting the cables across different floors of the building is known as the *vertical riser*, while the *horizontal interconnect* links desk computers and various systems on the same floor. And, the physical infrastructure of the central office managing intensive data applications and

information services is the *data center*.

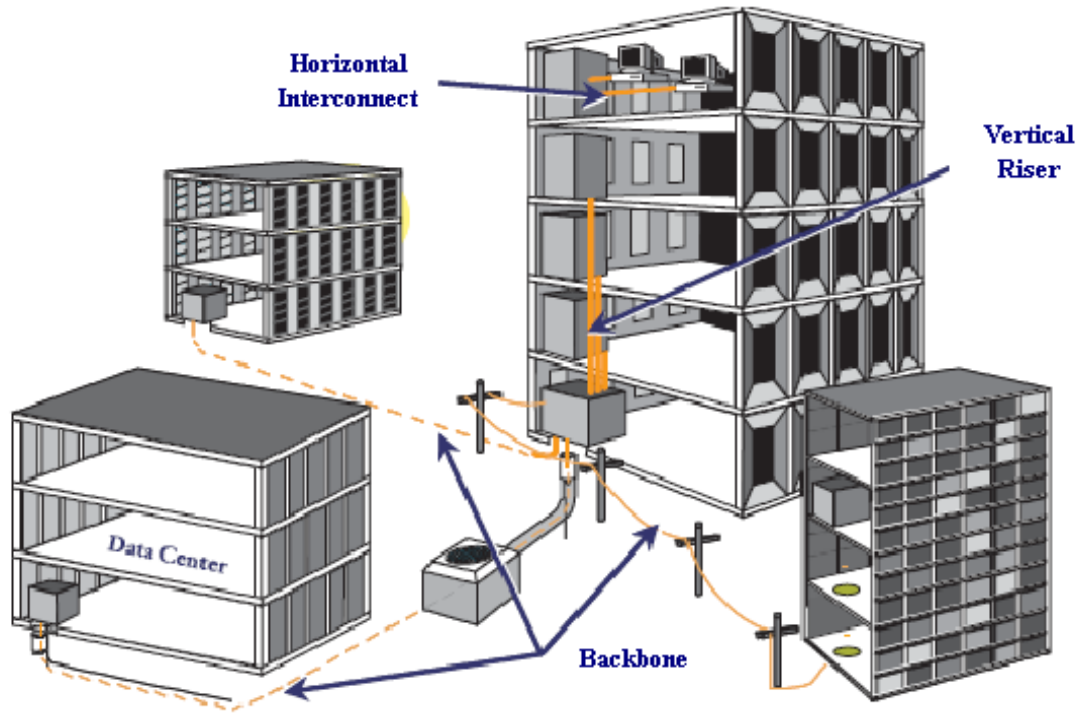


FIGURE 1.1. Premises network links

The backbones typically are optical fiber cables. The backbones usually are the longest links within a premises network and present the greatest challenge for higher data rates. The vertical riser links consist primarily of multi-mode fibers and the link lengths are shorter than the backbone spans. For very short reach applications, such as the horizontal interconnects and connections between electronic components in the data center, copper cables have dominated in the past. However, the demand for an ever increasing volume of data transmission such as Audio/Video, web conference, multimedia, and P2P applications, will max out the bandwidth of the current copper networks and make switching to optical fiber links a necessity. Fiber-optics will play an increasingly important role in the development of all types of links in premises networks.

1.2 Scope of Study

GbE and 10 GbE demand faster and lower cost optical sources to support the rapid modulation rates. 850 nm vertical cavity surface emitting lasers (VCSELs) and multimode fibers (MMFs) have long been the most cost effective choice for short reach premise applications as described in some detail in Chapter 2. Because the group velocity is not the same for different propagating modes in MMFs, the time for different modes to travel some fixed distance in the fiber varies, which causes modal dispersion. To better understand modal dispersion, a more thorough modal theory approach of the optical fiber is used in Chapter 3, and DMD measurements, a new method to characterize the modal dispersion of MMF is also introduced in Chapter 3. Different from light-emitting diodes (LEDs), a light source applied in Fast Ethernet at a lower modulation rate, VCSELs will underfill the fiber. The type of light source and how the light is coupled into the fiber affect the launch condition and MMF performance. Therefore, continuing to use an overfilled launch (OFL) condition to evaluate 850 nm VCSEL-based MMF systems may not be appropriate. In Chapter 4, an encircled flux launch condition is introduced, and the MMF macrobend loss performance is evaluated under both OFL and EFL conditions for comparison. Bandwidth characterization is an effective measurement to evaluate MMF modal dispersion. The impact of macrobending on MMFs bandwidth under different launch conditions is investigated in Chapter 5. 10 GbE optical links require a superior bandwidth to support high data rate capability. At the same time, the allowable margin in the 10 GbE link power budget is decreasing. The spare margin in an optical system can be used to extend the link distance, accommodate additional connectors or splices, or provide a safety margin for unplanned attenuation. It is more difficult for 10 GbE systems to support many tight bends of standard MMF, which makes it very challenging to build a MMF link that is also easy to install, low cost, and has a long life cycle. With current standard MMF fiber, it is possible to get into a situation where the 10 GbE

link margin is below zero, where the link will fail. In Chapter 6, the 10 GbE IEEE link model is applied to evaluate the impact of macrobending on the overall optical link performance. Finally, this dissertation concludes with a summary and possible future work in Chapter 7.

Chapter 2

10 GIGABIT ETHERNET FIBER-OPTICS

2.1 Optical Fiber Basics

As explained in [5][6][7][8], an optical fiber is a long, thin strand of very pure glass about the diameter of a human hair. It is a dielectric waveguide that transports electromagnetic energy at optical wavelengths. Although many different configurations of the optical waveguide have been discussed in the past [9], a fiber waveguide normally is in a cylindrical shape and consists of three coaxial layers as shown in Figure 2.1. The central region is the core of refractive index n_1 , surrounded by a cladding region which has a refractive index n_2 that is less than n_1 . The buffer coating is a protective layer to add further strength to the fiber and mechanically buffer the fiber from perturbations [6] which could cause scattering losses.

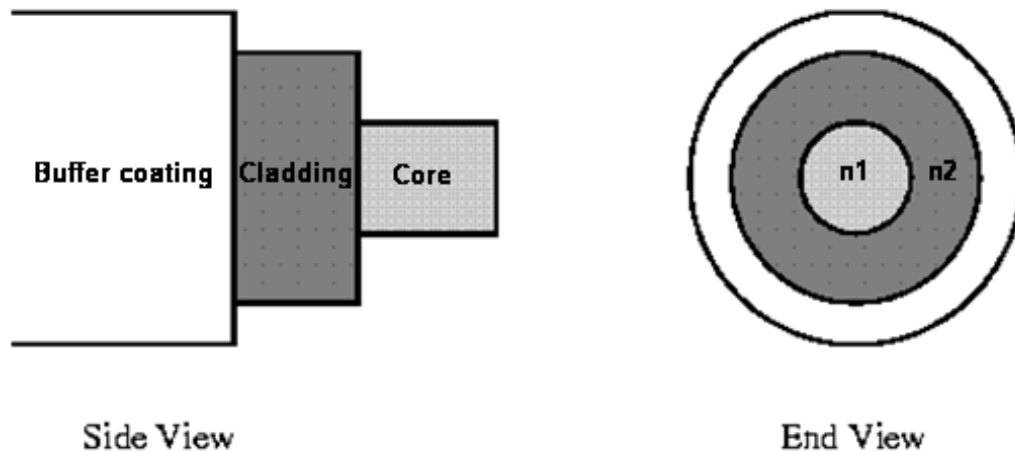


FIGURE 2.1. Schematic of a fiber structure

An important characteristic of fiber optics is refraction. When light passes from

one transparent material to another, it bends according to Snell's law which is defined as:

$$n_1 \sin(\theta_1) = n_2 \sin(\theta_2) \quad (2.1)$$

where n_1 is the refractive index of the medium the light is leaving, θ_1 is the incident angle between the light beam and the normal (normal is 90° to the interface between two materials). n_2 is the refractive index of the material the light is entering, and θ_2 is the refractive angle between the light ray and the normal.

When a light ray crosses an interface from a higher refractive index medium to a lower refractive index medium it will bend away from the normal. At some angle, known as the critical angle θ_c , light traveling from a higher refractive index medium to a lower refractive index medium will be refracted at 90° ; in other words, refracted along the interface. If the light hits the interface at any angle larger than this critical angle, it will not pass through to the second medium at all. Instead, all of it will be reflected back into the first medium, a process known as total internal reflection, which is illustrated in Figure 2.2.

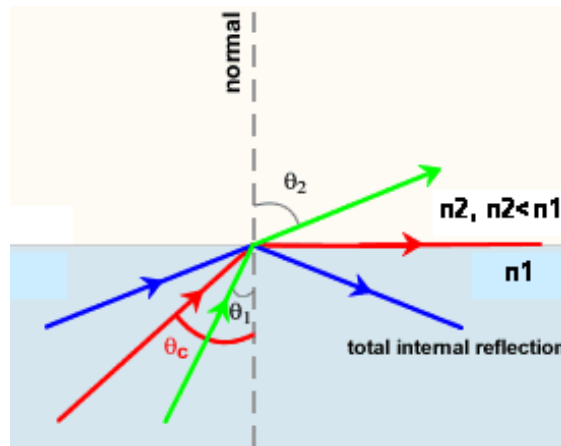


FIGURE 2.2. Refraction, critical angle and total internal reflection at a material boundary

Optical fibers are based entirely on the principle of total internal reflection (TIR). The core refracts the light and guides the light along its path. The cladding reflects any light back into the core and stops light from escaping through it. This is explained in the following Figure 2.3.

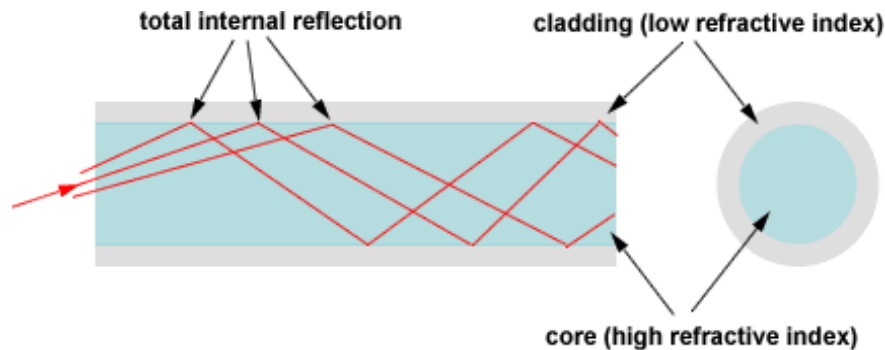


FIGURE 2.3. The propagation mechanism in an ideal step-index optical fiber

Although fibers can be made out of transparent plastic, glass, or a combination of the two, the fibers used in long-distance telecommunications applications are always glass because of the lower optical attenuation.

2.2 Single-mode Fiber and Multi-mode Fiber

There are two different types of optical fiber: single-mode and multi-mode.

2.2.1 Single-mode Fiber

A single-mode optical fiber is an optical fiber of a small core diameter designed to carry only a single mode which travels at the center of the core. The light stably passes through the length of fiber with low loss and retains the fidelity of each light pulse over long distances. For these reasons, single-mode fibers have high bandwidth and are used for long distance links. The core diameter of single-mode fiber is less than ten times the wavelength of the propagating light, typically around $9 \mu\text{m}$. It

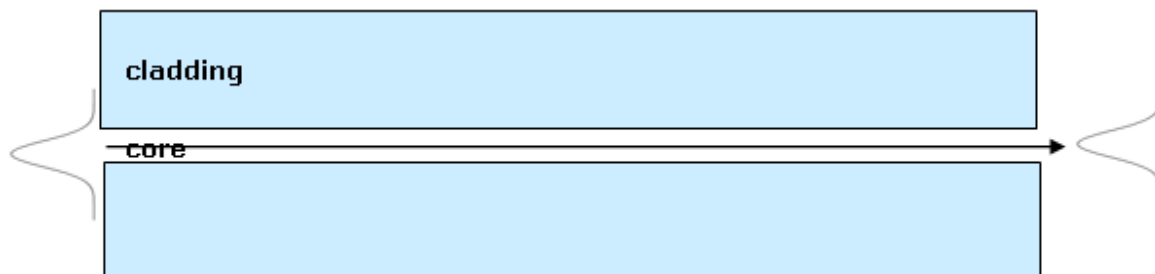


FIGURE 2.4. Single-mode fiber

requires tighter tolerances to couple light into and between single-mode fibers, and a laser source with good beam quality and precise alignment is needed to achieve mode matching. Single-mode transmitters, receivers, amplifiers, and other components are generally more expensive than multi-mode components, but the single-mode fiber itself, is usually cheaper than multi-mode fiber.

2.2.2 Multi-mode Fiber

Multi-mode fiber (MMF) has a large core diameter (from $50\ \mu\text{m}$ to $200\ \mu\text{m}$) that allows light to take multiple different paths, or modes, down the fiber. Rays of light entering the fiber at low angles travel faster along the fiber than those rays that enter at steeper angles and reflect many more times from the core/cladding boundaries as they travel through the fiber. Figure 2.5 shows light rays traveling through a step-index MMF. The arrival of different modes of the light at different times due to different mode velocities is called the modal dispersion.

A step-index MMF has a homogeneous core and the refractive index profile of the fiber is a step function as shown in Figure 2.6(b). In a step-index MMF an initially sharp pulse made up of many modes broadens due to modal dispersion. This limits the bit rate and distance for signal transmission because it determines how closely input pulses can be spaced without overlap at the fiber output. Such fibers are normally used for short distance conventional image transfer. A graded-index

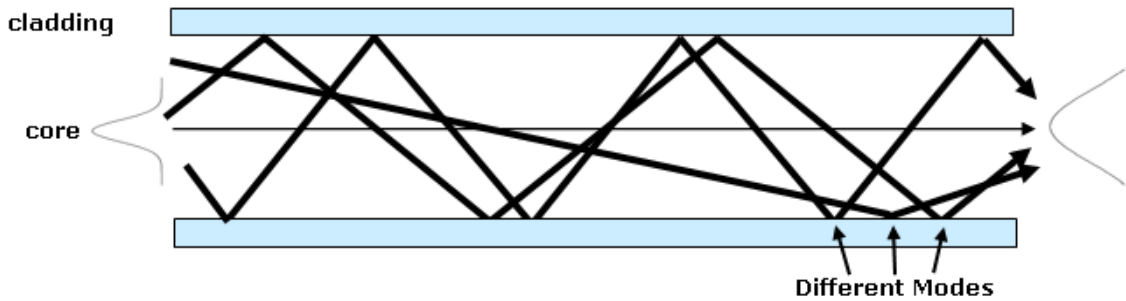


FIGURE 2.5. Step-index multimode fiber

MMF's refractive index decreases gradually away from its center, finally dropping to the same value as the cladding at the edge of the core. The refractive index profile shape of graded-index MMFs, as shown in Figure 2.6(c), is used to minimize pulse broadening. Since light travels more slowly in the high-index region of the fiber relative to the low-index region, significant equalization of the transit time for the various modes can be achieved to reduce pulse broadening. This type of fiber is suitable for intermediate-distance, intermediate-bit-rate transmission systems.

The comparison of single-mode fiber, step-index MMF and graded-index MMF is summarized in Figure 2.6.

As mentioned in §1.1 an optical fiber has higher bandwidth than a copper wire, so an optical fiber cable can save space in cable ducts because a single fiber can carry much more data than a single electrical cable. Also, optical fiber is immune to electrical interference, having no cross-talk between signals in different cables and no pickup of environmental noise. Fiber also has no electric conductivity, which makes it a good and safe solution in high-voltage environments or in environments where explosive fumes are present.

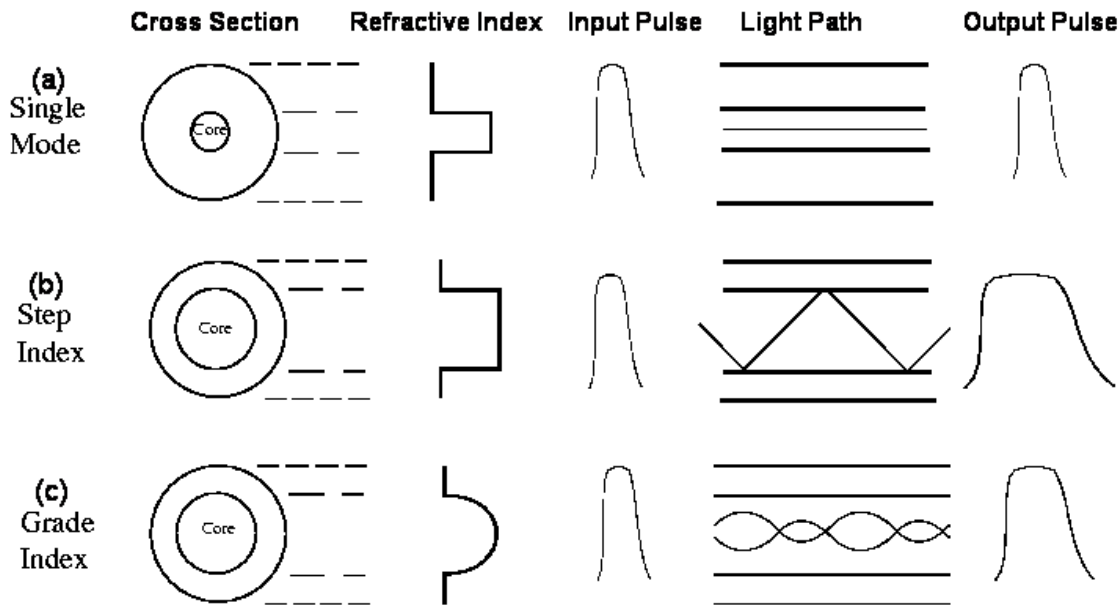


FIGURE 2.6. Comparison of types of optical fiber designs.(a) single-mode fiber, both stepped-index and graded-index are possible, (b) stepped-index MMF, (c) graded-index MMF.

2.3 Optical Transmitters

A transmitter is an electronic device or circuit that transmits analog or digital signals. For use in optical communications, transmitters generate the optical signal and must be designed to be compact, efficient, and reliable, while operating in an optimal wavelength range. Except for switching electronics[4], the optical transmitters are the most expensive part of a premises network installation. The switch electronics are independent of fiber type and, therefore, changes in transmitter cost will have the greatest effect on overall network costs. The demand for ever increasing volume of data transmission is driving new development not only for faster but also lower cost optical transmitters.

There are four main types of optical transmitters that can be used in optical communication networks. These light sources differ greatly in cost, optical characteristics, and performance. Distributed feedback (DFB) and Fabry-Perot (FP) lasers are ex-

pensive relative to light-emitting diodes (LEDs) and vertical cavity surface emitting lasers (VCSELs). DFB and FP lasers produce a highly focused coherent single mode beam with high power, which allows efficient coupling of power into the small core of single-mode fiber. LEDs and VCSELs offer an inexpensive solution for short-reach applications, like premises networks, but are unsuitable for single-mode fiber since LEDs create incoherent light, and VCSELs create multi-mode laser beams so only a small portion of the light can be coupled into a single-mode fiber, or the coupling efficiency is too low. Therefore large core MMF should be used in combination with LEDs and VCSELs to benefit from their cost advantage.

LEDs are used for Fast Ethernet (10Mbps-100Mbps). The LED modulation rate is limited to about 622 Mbps, so they are not applied for GbE or 10 GbE. Since 850 nm VCSELs can easily operate at speeds beyond Gbps and produce milliwatts of power with very low threshold currents, 850 nm VCSELs have become the choice for short-reach premises applications.

Single-mode fiber is not designed to operate at 850 nm whereas MMF is able to work at that wavelength for short-reach applications. The initial cost of MMF is higher than single-mode fiber, but the large core of MMF (five times larger diameter than a single-mode fiber) enables low loss connection and simple transmitter-to-fiber or fiber-to-fiber alignment. So the use of MMF together with low cost 850 nm VCSELs can reduce the overall cost of premise network installations. The system cost of the MMF and VCSEL solution is about half that of the single-mode fiber and FP laser solution[10]. Also VCSELs have a broad data rate operating range from 10 Mbps up to 10 Gbps, and thus can provide customers with a variety of network data rates on the same fiber. Therefore, the combination of MMF and 850 nm VCSELs constitutes a cost-effective solution for current and future data-communication needs.

Chapter 3

MODAL DISPERSION IN MULTIMODE FIBER

In Chapter 2, MMF and single-mode fiber are illustrated using simplified geometrical ray optics. To better understand the optical fiber, the electromagnetic wave or modal theory approach must be used.

3.1 Modes in Optical Fibers

Optical fibers are circular dielectric waveguides in which a discrete set of electromagnetic fields can propagate within the fiber core. Those fields are the modes in optical fibers. The modal fields depend on the refractive index profile, the cross section geometry, and the frequency of the light source. The normalized frequency, or the V number, is defined by those parameters:

$$V = \frac{2\pi a}{\lambda} \sqrt{n_{co}^2 - n_{cl}^2} \quad (3.1)$$

where a is the core radius, λ is the wavelength in vacuum, n_{co} is the maximum refractive index of the core, n_{cl} is the refractive index of the homogeneous cladding.

Another important property is the numerical aperture, or N.A., which is defined as the sine of the half-angle of the maximum cone an incident ray can have for TIR in the core. It can be expressed as:

$$N.A. = n \sin \theta_{\max} = \sqrt{n_{co}^2 - n_{cl}^2} \quad (3.2)$$

N.A. is a measure of how easy it is to couple light into a fiber. The normalized index difference is defined as:

$$\Delta = \frac{n_{co}^2 - n_{cl}^2}{2n_{co}^2} \quad (3.3)$$

The V number can also be express in $N.A.$ and Δ as:

$$V = \frac{2\pi a}{\lambda} \cdot N.A. = \frac{2\pi a}{\lambda} \cdot n_{co} \sqrt{2\Delta} \quad (3.4)$$

Electromagnetic wave propagation along optical fibers follows Maxwell's equations, which can be reformed into the vector Helmholtz wave equations. For example, consider a step index fiber where

$$n(r) = \begin{cases} n_{co}, & r < a \\ n_{cl}, & r \geq a \end{cases} \quad (3.5)$$

where again a is the core radius.

The refractive index is independent along the propagation z direction. The field solutions of the wave equations can be written in the form [11]:

$$\begin{aligned} E(r, \phi, z) &= E_0(r, \phi) \exp(-j\beta z) \\ H(r, \phi, z) &= H_0(r, \phi) \exp(-j\beta z) \end{aligned} \quad (3.6)$$

where radius r , the azimuthal angle ϕ and z are the three cylindrical coordinates used when the fiber axis coincides with the z axis. β is the propagation constant of the fiber mode in z direction. The restriction on β is:

$$n_{cl}k_0 < \beta < n_{co}k_0 \quad (3.7)$$

to keep the mode propagation inside optical fiber, where $k_0 = \frac{2\pi}{\lambda}$ is the free space propagation constant.

The z component of E can be expressed using the cylindrical coordinates:

$$\nabla_t^2 E_{zco} + (n_{co}^2 k_0^2 - \beta^2) E_{zco} = 0 \quad r \leq a \quad (3.8)$$

$$\nabla_t^2 E_{zcl} + (n_{cl}^2 k_0^2 - \beta^2) E_{zcl} = 0 \quad r > a \quad (3.9)$$

and the solution for E_z in terms of Bessel functions takes the form [11]:

$$E_z = \begin{cases} A J_q(ur/a) \sin(q\phi + \alpha) \exp(-j\beta z) & r \leq a \\ C K_q(wr/a) \sin(q\phi + \alpha) \exp(-j\beta z) & r \geq a \end{cases} \quad (3.10)$$

where

$$u = a(n_{co}^2 k_0^2 - \beta^2)^{\frac{1}{2}} \quad (3.11)$$

is the normalized transverse propagation constant, and

$$w = a(\beta^2 - n_{cl}^2 k_0^2)^{\frac{1}{2}} \quad (3.12)$$

is the normalized transverse attenuation constant; q is the angular or azimuthal mode number, and it must be an integer in order to maintain the field self-consistent on each rotation of ϕ through 2π ; J_q and K_q are ordinary and modified Bessel functions of the first kind, and of order q ; α is a constant phase shift.

The z component of H can be resolved in the same way as [11]:

$$H_z = \begin{cases} B J_q(ur/a) \cos(q\phi + \alpha) \exp(-j\beta z) & r \leq a \\ D K_q(wr/a) \cos(q\phi + \alpha) \exp(-j\beta z) & r \geq a \end{cases} \quad (3.13)$$

Similarly, the transverse field components are resolved as:

$$E_r = \begin{cases} \left[-A \frac{j\beta}{(u/a)} J_q'(ur/a) + B \frac{j\varpi\mu}{(u/a)^2} \frac{q}{r} J_q(ur/a) \right] \sin(q\phi + \alpha) \exp(-j\beta z) & r \leq a \\ \left[C \frac{j\beta}{(w/a)} K_q'(wr/a) - D \frac{j\varpi\mu}{(w/a)^2} \frac{q}{r} K_q(wr/a) \right] \sin(q\phi + \alpha) \exp(-j\beta z) & r \geq a \end{cases} \quad (3.14)$$

where ϖ is the radian frequency, and μ is the permeability tensor, and:

$$H_r = \begin{cases} \left[A \frac{j\varpi\epsilon_0 n_{co}^2}{(u/a)^2} \frac{q}{r} J_q(ur/a) - B \frac{j\beta}{(u/a)} J_q'(ur/a) \right] \cos(q\phi + \alpha) \exp(-j\beta z) & r \leq a \\ \left[-C \frac{j\varpi\epsilon_0 n_{cl}^2}{(w/a)^2} \frac{q}{r} K_q(wr/a) + D \frac{j\beta}{(w/a)} K_q'(wr/a) \right] \cos(q\phi + \alpha) \exp(-j\beta z) & r \geq a \end{cases} \quad (3.15)$$

where ϵ_0 is the free space permittivity, and:

$$E_\phi = \begin{cases} \left[-A \frac{j\beta}{(u/a)^2} \frac{q}{r} J_q(ur/a) + B \frac{j\varpi\mu}{(u/a)} J'_q(ur/a) \right] \cos(q\phi + \alpha) \exp(-j\beta z) & r \leq a \\ \left[C \frac{j\beta}{(w/a)^2} \frac{q}{r} K_q(wr/a) - D \frac{j\varpi\mu}{(w/a)} K'_q(wr/a) \right] \cos(q\phi + \alpha) \exp(-j\beta z) & r \geq a \end{cases} \quad (3.16)$$

$$H_\phi = \begin{cases} \left[-A \frac{j\varpi\epsilon_0 n_{co}^2}{(u/a)} J'_q(ur/a) + B \frac{j\beta}{(u/a)^2} \frac{q}{r} J_q(ur/a) \right] \sin(q\phi + \alpha) \exp(-j\beta z) & r \leq a \\ \left[C \frac{j\varpi\epsilon_0 n_{cl}^2}{(u/a)} K'_q(wr/a) - D \frac{j\beta}{(w/a)^2} \frac{q}{r} K_q(wr/a) \right] \sin(q\phi + \alpha) \exp(-j\beta z) & r \geq a \end{cases} \quad (3.17)$$

From equations 3.10 to 3.17 above, when $q = 0$ and $A = C = 0$, there is no z and r components of electric field, no ϕ component of magnetic field, and only the transverse electric modes with nonzero components H_z , H_r and E_ϕ arise. Those modes are therefore called TE_{0m} modes, where $q = 0$ is the mode order; m is the radial mode order, and $m \geq 1$. Similarly, when $q = 0$, $B = D = 0$, only the transverse magnetic modes with nonzero E_z , E_r and H_ϕ exist, and are called TM_{0m} modes. When $q \neq 0$, it physically corresponds to *skew* rays which propagate in the fiber core in a spiral pattern and never come across the z axis; thus, the modes have z components for both the electric and magnetic fields. As a result, those modes are called hybrid modes, and are designated HE_{qm} or EH_{qm} .

By applying all boundary continuity conditions and the weakly guiding approximation [12] simplification, i.e., when $n_{co} \approx n_{cl}$, the modes eigenvalue equation can be derived:

$$u \frac{J_{l-1}(u)}{J_l(u)} = -w \frac{K_{l-1}(w)}{K_l(w)}, \quad l = \begin{matrix} 1 & TE_{0m}, TM_{0m} \\ q+1 & EH_{qm} \\ q-1 & HE_{qm} \end{matrix} \quad (3.18)$$

where l is an integer.

Typically n_{co} is very close to n_{cl} , and the normalized index difference can also be expressed applying this weakly guiding approximation:

$$\Delta \approx \frac{n_{co} - n_{cl}}{n_{co}} = \frac{\delta n}{n_{co}} \quad (3.19)$$

A typical value of Δ for single-mode fiber is $\sim 0.35\%$, a typical value for MMF is $\sim 1\%$.

From equations 3.1, 3.11, and 3.12, the V number can also be expressed as:

$$V = \sqrt{u^2 + w^2} = \frac{2\pi a}{\lambda} \cdot n_{co} \sqrt{2\Delta} \quad (3.20)$$

Equations 3.18 and 3.20 are often used to determine the cutoff conditions for the modes by setting $w = 0$ in the two equations, which leads to

$$V \frac{J_{l-1}(V)}{J_l(V)} = 0 \quad (3.21)$$

When $V = 0$, equation 3.21 is handled by the small argument approximation [11]:

$$V \frac{J_{l-1}(V)}{J_l(V)} \approx \frac{lV(V/2)^{l-1}}{(V/2)^l} = 2l = 0 \quad (3.22)$$

which leads to $l = 0$, and $V \frac{J_{-1}(V)}{J_0(V)} = 0$.

When $V \neq 0$, equation 3.21 can be simplified as:

$$J_{l-1}(V) = 0, \quad V \neq 0 \quad (3.23)$$

Using equation 3.23 above, each Bessel ordinary function zero is identified at a value of V , and each TE_{0m} , TM_{0m} , EH_{qm} , or HE_{qm} mode with cutoff happening at that V number is also determined. Most modes are degenerate, such as modes TE_{01} , TM_{01} and HE_{21} all have the same cutoff condition at $V = 2.405$. Thus, the LP (Linearly Polarized) modes system is used for degenerated sets of modes under the weakly guiding approximation.

LP mode intensity

The LP_{lm} modes are identified using the cutoff condition equation 3.23, for example the LP_{11} set is identified at the first Bessel function zero at $V = 2.405$, which

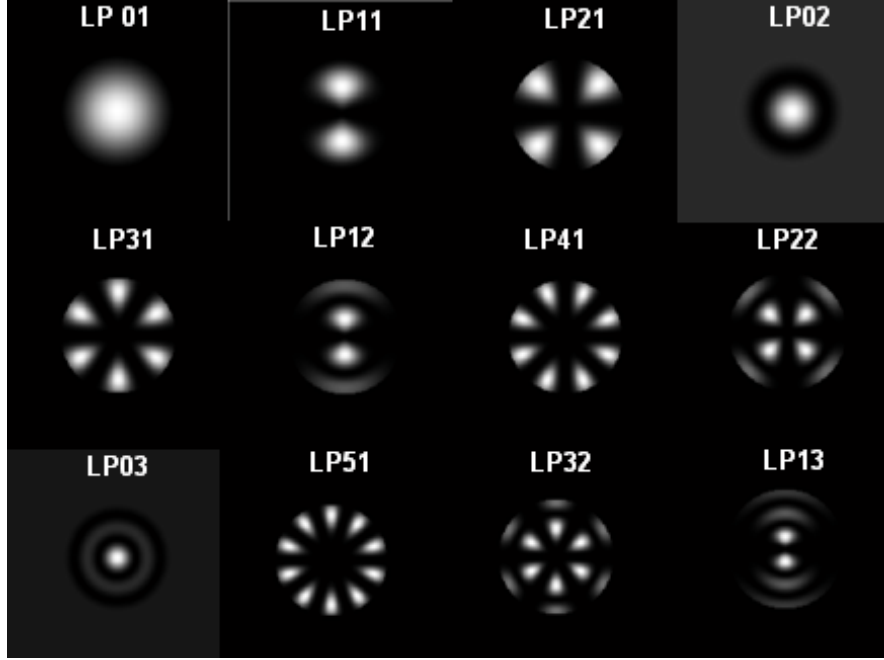


FIGURE 3.1. Matlab simulation of intensity distribution of first 12 LP modes in a step-index fiber

corresponds to the TE_{01} , TM_{01} and HE_{21} modes above. Using Matlab, the intensity distributions of the first 12 LP modes in a step-index fiber were generated considering the cutoff conditions, where [11]

$$\begin{aligned} I_{lm} &= I_0 J_l^2\left(\frac{ur}{a}\right) \sin^2(l\phi) & r \leq a \\ I_{lm} &= I_0 \left(\frac{J_l(u)}{K_l(w)}\right)^2 K_l^2\left(\frac{wr}{a}\right) \sin^2(l\phi) & r \geq a \end{aligned} \quad (3.24)$$

and I_0 is the peak intensity. The simulation results are listed in Figure 3.1.

The normalized propagation constant b is another useful property and is defined as:

$$b = 1 - \frac{u^2}{V^2} = \frac{\beta^2 - n_{cl}^2 k_0^2}{n_{co}^2 k_0^2 - n_{cl}^2 k_0^2} = \frac{n_{eff}^2 - n_{cl}^2}{n_{co}^2 - n_{cl}^2} \quad (3.25)$$

where

$$n_{eff} \equiv \frac{\beta}{k_0} \quad (3.26)$$

is the effective guide index. In reference[13], normalized propagation constant b as a

function of the normalized frequency V was introduced, and a similar plot is presented in Figure 3.2.

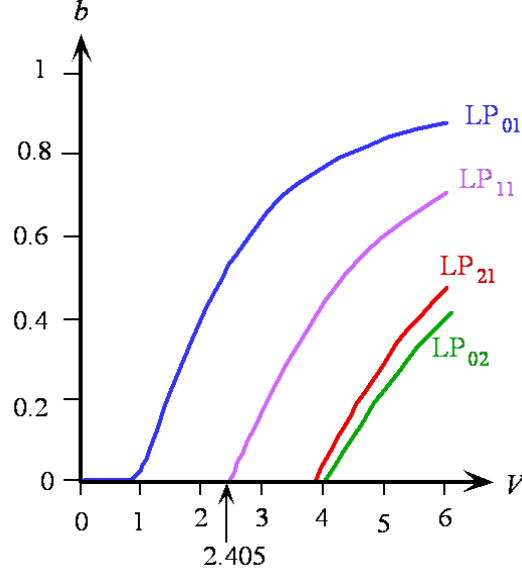


FIGURE 3.2. Normalized propagation constant b as a function of V

Single-mode fibers are designed to allow only one electromagnetic mode, LP_{01} , to propagate in the fiber. This mode is therefore also called fundamental mode. The normalized frequency of a single-mode fiber needs to meet the criterion: $V = \frac{2\pi a}{\lambda} \cdot N.A. < 2.405$.

For MMFs, the refractive index profile can be expressed in more general terms:

$$n(r) = \begin{cases} n_{co}\sqrt{1 - 2\Delta\left(\frac{r}{a}\right)^\alpha}, & r < a \\ n_{co}\sqrt{1 - 2\Delta} = n_{cl}, & r \geq a \end{cases} \quad (3.27)$$

where α is the curvature parameter of the core, and it is chosen to optimize the MMF performance. $\alpha = 2$ corresponds to a parabolic graded index profile, $\alpha = \infty$ corresponds to a step index profile.

When a large number of modes propagate inside a fiber waveguide, or $V \gg 1$, using the WKB approximation [14], the mode volume or the number of bound modes

that the fiber can support is approximately:

$$N \approx \frac{V^2}{2} \left(\frac{\alpha}{\alpha + 2} \right) \quad (3.28)$$

3.2 Attenuation and Dispersion

3.2.1 Attenuation

Also known as transmission loss, attenuation is a reduction in the transmitted power [15] propagating in a fiber. For silica fiber, attenuation is very low as compared to other transmission media (i.e., copper, coaxial cable, etc.). It depends strongly on the wavelength. For standard single-mode fibers, a typical attenuation value at 1300 nm is 0.35 dB/km, and the lowest attenuation is near 1550 nm with a typical value of 0.2 dB/km. For standard MMFs operate at 850 nm with a typical value of 2.3 dB/km. The light power decays exponentially with length due to *absorption*, *scattering losses* and *bending losses*.

3.2.2 Dispersion

Dispersion is the spreading of the optical pulses as they travel through the fiber. Dispersion in optical fibers can be categorized into three main types.

The first type is *material* dispersion. This type of intramodal dispersion results from the fact that the refractive index of the fiber varies as a function of wavelength [6], so different wavelengths will travel through an optical fiber at different velocities. It also depends on the source line width, so for long distance communications links, it is desirable to use a laser with a very narrow linewidth such as a DFB discussed in Chapter 2.

The second type of dispersion is *waveguide* dispersion which results from the fact that the signal in the cladding travels with a higher velocity than the signal in the core. Its magnitude depends on the shape, design, and chemical composition of the

fiber core, and is significant in single-mode fiber. Waveguide dispersion can be altered by changing the fiber refractive index profile.

The final type of dispersion is *modal* dispersion, or *intermodal* dispersion. It only exists in MMF since it is a phenomenon between different modes in an optical fiber. Because the group velocity is not the same for different propagating modes, the time it takes each mode to travel some fixed distance varies for the different modes. The intermodal dispersion limits both the data transmission rate of a MMF as well as the distance it can transport data. It can be altered by optimizing the α profile parameter discussed in equation 3.27.

3.2.3 Effects of Dispersion and Attenuation

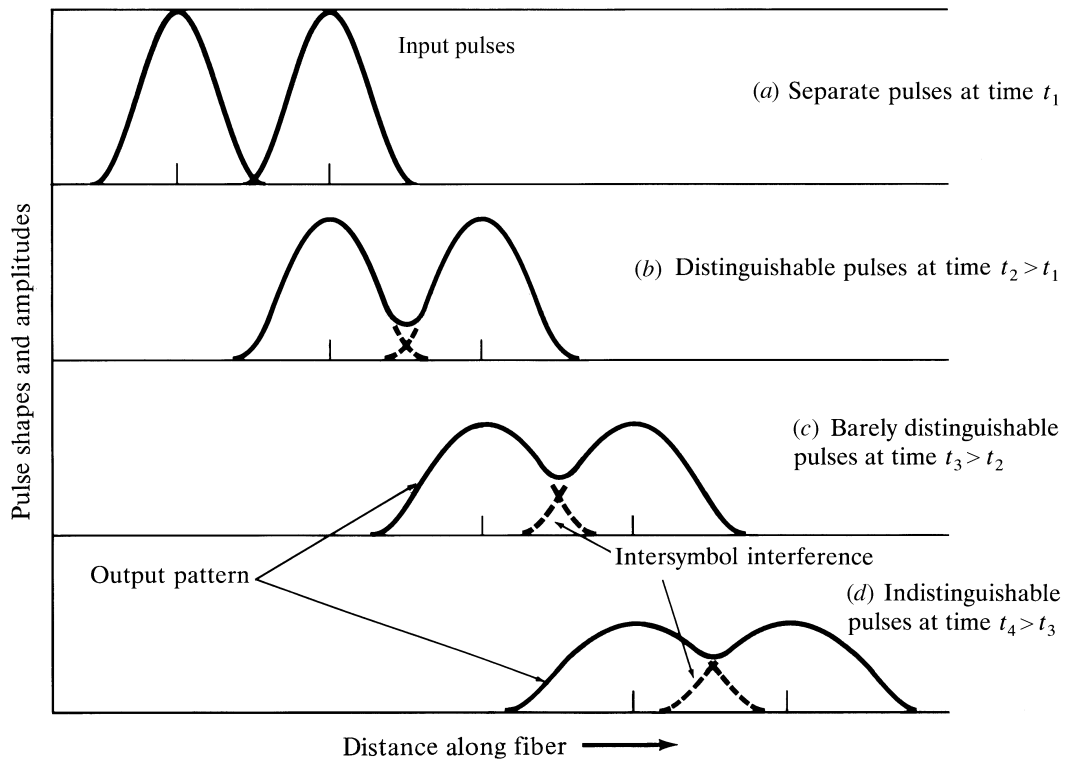


FIGURE 3.3. Effects of dispersion and attenuation

As illustrated in Figure 3.3[16], after traveling a distance along the fiber, the input pulse amplitudes decrease due to attenuation, and the pulses begin to overlap and the symbols finally become indistinguishable due to the dispersion.

3.3 Intermodal Dispersion Measurement

3.3.1 MMF Mode Groups

Fiber mode propagation in a MMF is much more complicated than in a single-mode fiber due to the intermodal dispersion. Using equations 3.4 and 3.28, a typical 50 μm parabolic graded index MMF at 850 nm wavelength can support about 400 modes. However, as discussed in Chapter 6 of reference [11], in some cases the propagation constants β or the normalized propagation constants b are very close for a certain group of modes. Those modes can be grouped into one mode group (MG). All the propagating modes can be divided into degenerate MGs by the principle mode number p defined in [17] as:

$$p = 2m + l - 1 \quad (3.29)$$

and there are about $\text{mod}[(p+1)/2]$ modes in MG p [18]. So the 400 modes in a typical MMF discussed above can be grouped into about 20 MGs. In a low bandwidth (see Chapter 5 for definition) MMF, those MGs will spread out in time considerably due to intermodal dispersion.

3.3.2 Differential Mode Delay Measurement

Intermodal dispersion can be evaluated using the differential mode delay (DMD) method [19]. In a DMD measurement, a single mode laser light pulse through a single-mode fiber ($\sim 5 \mu\text{m}$ spot size) is scanned across the 50 μm core of the MMF under test at 2 μm increments as illustrated in Figure 3.4. At each radial position,

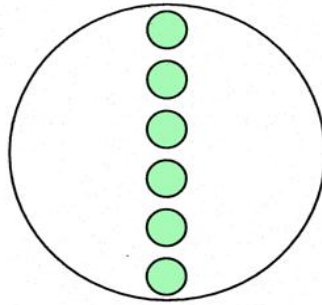


FIGURE 3.4. Differential modal delay measurement scan

the input pulse excites different MGs within a MMF, and the delay of each MG is measured and stored.

The superposition of all the delays at different radial locations provides a complete and detailed DMD trace as shown in Figure 3.5.

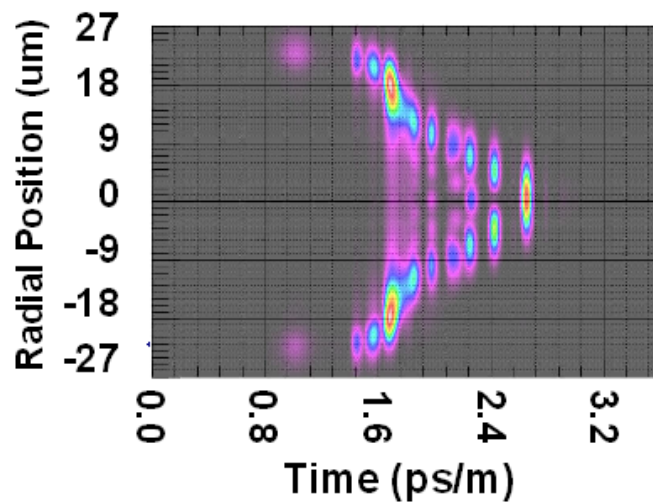


FIGURE 3.5. DMD measurement result of standard MMF1

The color scale from red to purple represents the power intensity of MGs from high to low. The Y axis is the radial position of the offset launch, where "0" indicates

the center of the MMF core. The X axis is the delay time normalized by the length of the fiber under test, where "0" is an arbitrary reference time. From Figure 3.5, standard MMF1 has a large spread in the delays between the outer and inner MGs at large and small radial offsets, respectively. The outer MGs, also the higher order MGs, tend to lead, resulting in a backwards 'C' delay pattern.

The DMD trace for standard MMF2 shown in Figure 3.6, on the other hand, has very low relative delays between most MGs except for the very outer MGs at about $23 \mu\text{m}$ radius. Still the spread in the delays is much smaller compared to standard MMF1, which also indicates that the bandwidth (see Chapter 5 for definition) of standard MMF2 is much higher than that of standard MMF1.

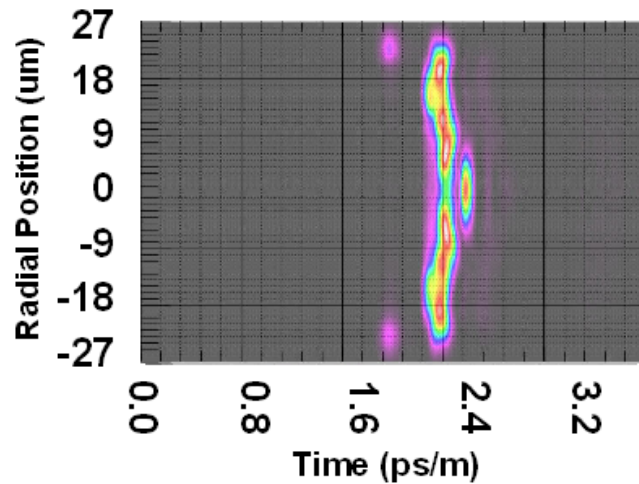


FIGURE 3.6. DMD measurement result of standard MMF2

Chapter 4

MULTIMODE FIBER LAUNCH CONDITIONS

4.1 Overfilled Launch (OFL) and Laser Source Launch

As discussed in §2.3, different types of optical transmitters can be very different in cost, optical characteristics, and performance. Therefore, the type of light source used for the link and the way it is coupled into the fiber greatly affects the choice of launch conditions.

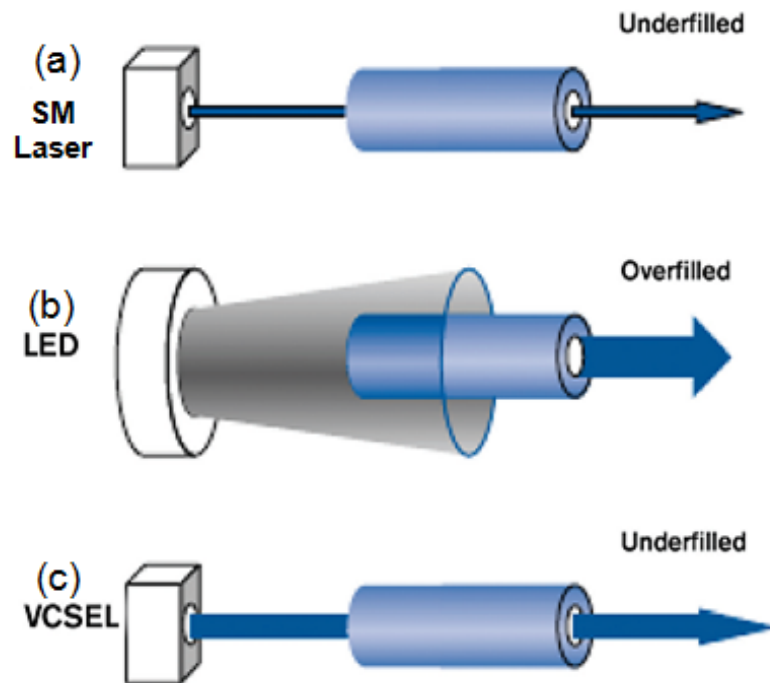


FIGURE 4.1. Launch conditions for commonly used fiber-optic light sources

Generally[20], lasers for single-mode fiber (DFB and FP) have a small spot di-

ameter and numerical aperture, which means they significantly underfill the fiber as shown in Figure 4.1(a). The light emitted by LEDs is incoherent and covers a greater spectral range, which leads to larger numerical aperture, greater dispersion, and poor coupling performance. As presented in Figure 4.1(b), an LED overfill the fiber. VCSELs typically have a small numerical aperture, with a larger spot diameter of about 15 μm and low source power, which makes VCSELs also unsuitable for coupling light into single-mode fiber. However, VCSELs underfill MMF (Figure 4.1(c)) as DFB and FP lasers underfill single-mode fiber.

Originally, MMF systems were designed for use in LED-based links operating at low bit rates of 10-100 Mbps. The MMFs performance, such as attenuation and bandwidth (see Chapter 5 for definition), was characterized based on an overfilled launch (OFL)[21] condition, which introduced nearly equal power into every mode to accurately simulate the launch condition of LEDs. As underfilled VCSELs have become a widely used light source for MMF systems, light is only launched into a fraction of the fiber's available mode groups. Thus, using OFL to evaluate 850 nm VCSEL-based MMF systems can produce inaccurate, inconsistent, and misleading results. Therefore, the specifications[22] for VCSEL transmitter encircled flux (EF) was developed by the Telecommunication Industry Association (TIA) to ensure better consistency between the mode groups filled during characterization and the ones filled in the network application using VCSELs.

4.2 Encircled Flux Launch (EFL)

EF is defined [23] as the percentage of power within a given radius when light is launched by a transmitter into a MMF. Variations in VCSELs power distribution (see Figure 4.2 [24]) are potentially great, especially for VCSELs from different manufacturers. Therefore it is critical to specify the launch conditions used during characterization to ensure the consistent performance of 10 GbE links. The TIA FO

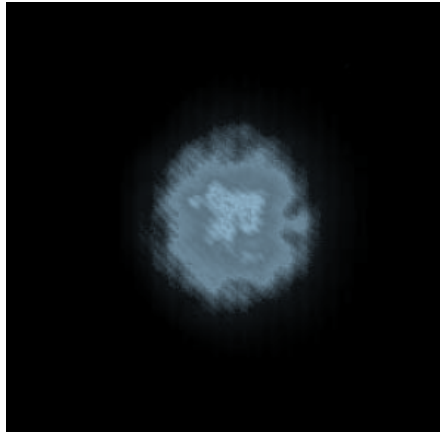


FIGURE 4.2. VCSEL near-field power distribution pattern

4.2.1 task group set boundary conditions on the allowable encircled flux for 850 nm VCSELs for a 10 GbE link as illustrated in Figure 4.3:

1. No more than 30 percent of the power is contained within $4.5 \mu\text{m}$ radius;
2. More than 86 percent of the power is contained within $19 \mu\text{m}$ radius.

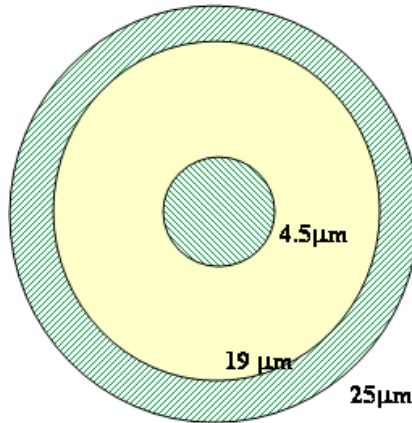


FIGURE 4.3. VCSEL EF boundary conditions specified for 10 GbE

Tom A. Hanson gave more details in his report [25] on the EF limit and the target EF was built using Laguerre/Hermite – Gaussian polynomials for the individual mode fields. Also in this report, various diameter mandrels with various numbers to launch

into standard OM3 [26] MMF were tried to get an EF radial curve as close to the target as possible. The condition producing an EF close to the target for MMF of 50 μm core diameter at 850 nm was found to be one turn at 25 mm diameter which is the red curve in Figure 4.4 [25].

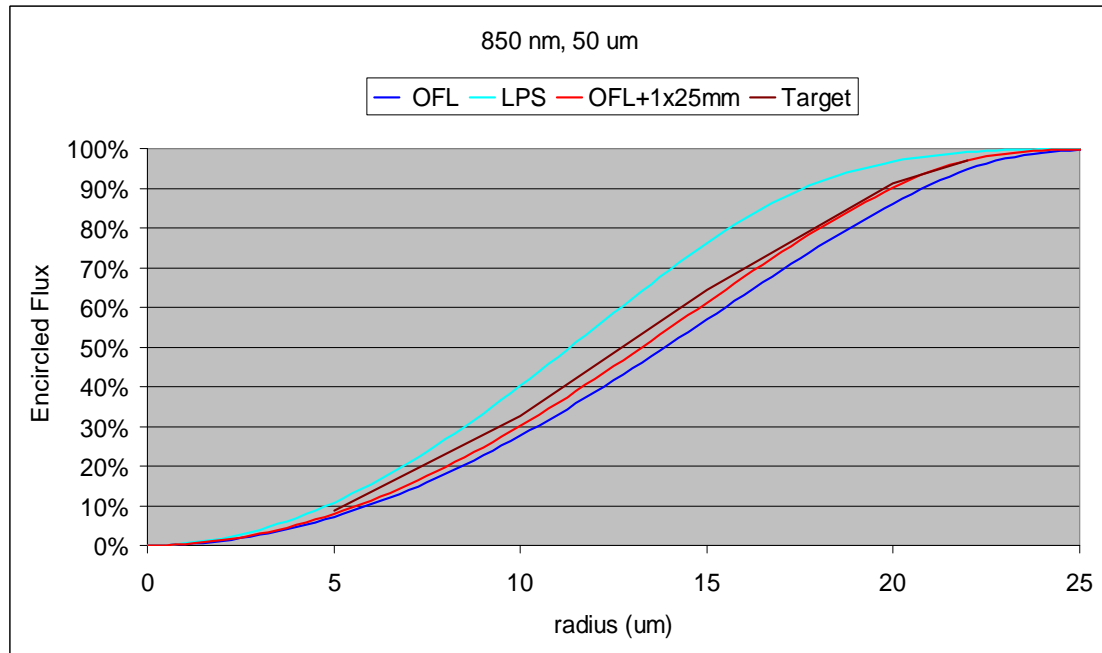


FIGURE 4.4. EF Curves for nominal OFL, LPS and Target EF for 50 μm fibers from Tom A. Hanson's report

This EFL condition was verified by testing the mode group powers at near-field of a standard OM3 MMF, which has a 50 μm core diameter, with both OFL and EFL defined as above. The results presented in Figure 4.5 show that peak power shifts from MG 15 & MG16 with OFL to MG 13 & MG 14 with EFL, and the power shifts towards the median radius MGs, and the highest outer radius MG power drops from above 7% to about 3.5% of the total power. This launch condition is indeed close to the EF target, so it was applied to the later studies as well.

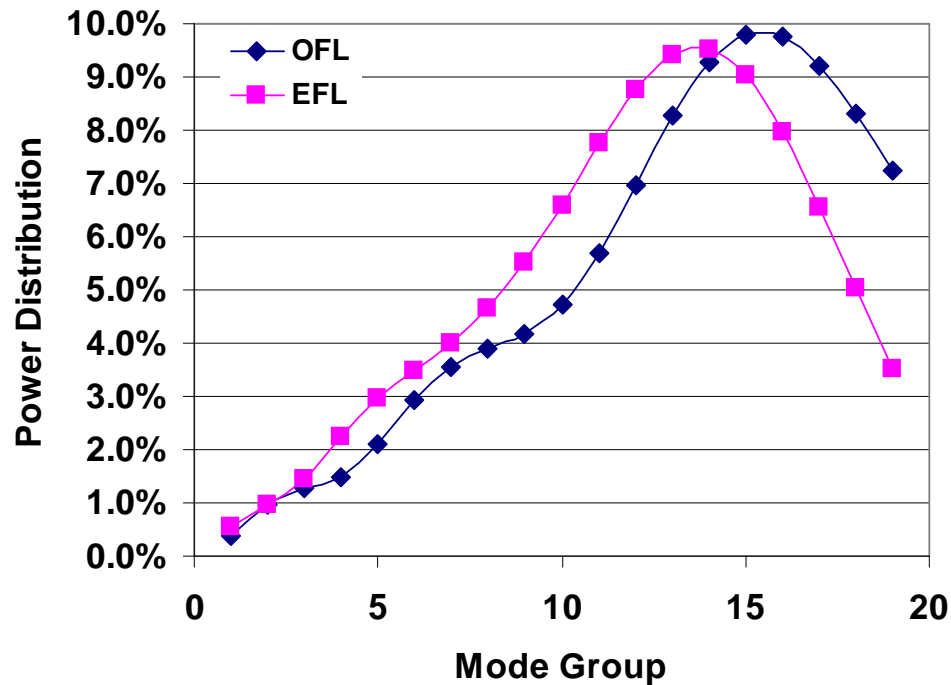


FIGURE 4.5. Mode groups power distribution at near-field of a standard OM3 MMF with OFL and EFL

4.3 MMF Macrobend Loss with OFL and EFL

As briefly mentioned in §3.2.1, bend loss is one of the major causes of fiber attenuation, resulting from bending a fiber or due to microscopic fiber deformation. The first type is called macrobending typically caused by cable handling or installation. The second type is generally referred to as microbending induced by external perturbations commonly occurring during the cabling and deployment of the fiber. The focus of this study is on macrobending when fiber is bent with a large radius relative to the fiber diameter.

As shown in Figure 4.6 [16], macrobends change the local fiber waveguide geometry. When the TIR condition fails, the propagating ray will transmit at an incident angle θ' or have a greater cladding penetration. From a mode field point of view, in

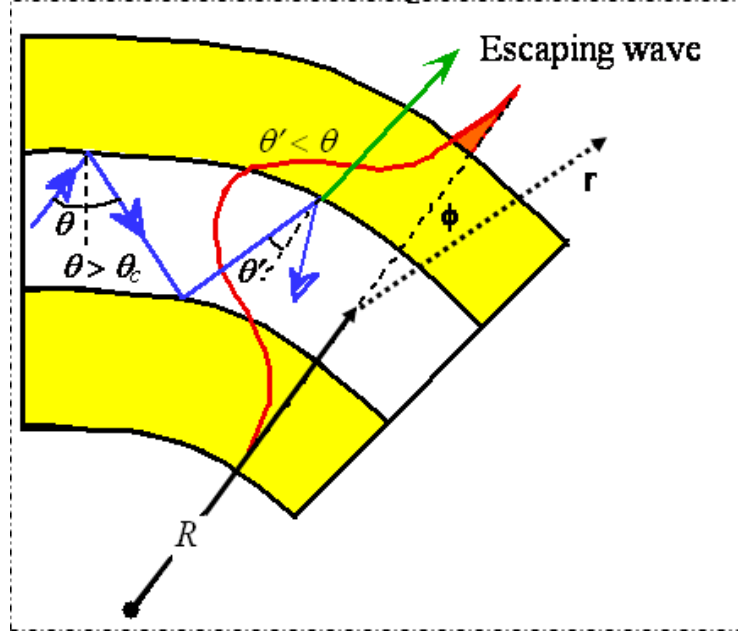


FIGURE 4.6. Macrobend loss occurs where TIR fails, and a portion of the mode field escapes.

order to maintain a wavefront perpendicular to the direction of propagation, modes at the outer bend radius are forced to travel faster than the modes at inner bend radius. When the mode velocity approaches the velocity of light in the cladding material, the mode energy in the outer mode field is lost through radiation [27]. The macrobending also leads to a decrease of the propagation constant β and n_{eff} as defined in Equation 3.26 for MGs at outer bend radius. The bent fiber can be described as an equivalent fiber with no bending with a modified index profile $n_{eff}(r, \phi)$ as [28][1]:

$$n_{eff}^2(r, \phi) = n^2(r, \phi) \cdot \left(1 + 2 \frac{r}{\rho R} \cos \phi\right) \quad (4.1)$$

where $n(r, \phi)$ is the refractive index of the same fiber with no bend, R is the bend radius, and r is the radial position from center of the core, ϕ is the local azimuth angle. And the elastooptics coefficient ρ is a constant that models the mechanical stress due to bending.

The higher order MGs of MMFs tend to travel closer to the edge of the fiber core and not too far from the cutoff condition. When a MG's n_{eff} is equal to n_{cl} , that MG is completely stripped out, which increases the optical attenuation. A recent study [1] characterized the macrobend loss of MMF only with OFL and restricted mode offset launch [22] conditions. The macrobend loss measurements of fiber samples with both OFL and EFL were conducted to evaluate the impact of launch conditions on MMFs bend loss performance in this study.

4.3.1 Experimental Setup

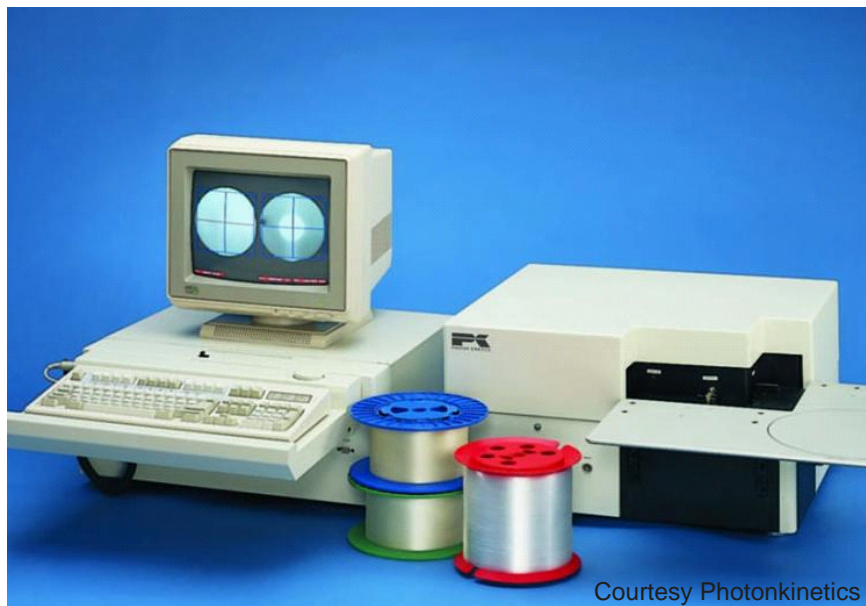


FIGURE 4.7. PK 2500 fiber analysis system

A commercially available spectral attenuation test bench, the PK 2500 fiber analysis system shown in Figure 4.7, was used to perform the macrobend loss measurements. A macro program was developed to execute the required operational commands of the bench. The spectral scans were accomplished by using a broad-band lamp source followed by a monochromator and other optical components to simulate

the OFL launch condition to the fiber under test (FUT). The FUT was about two meters long.

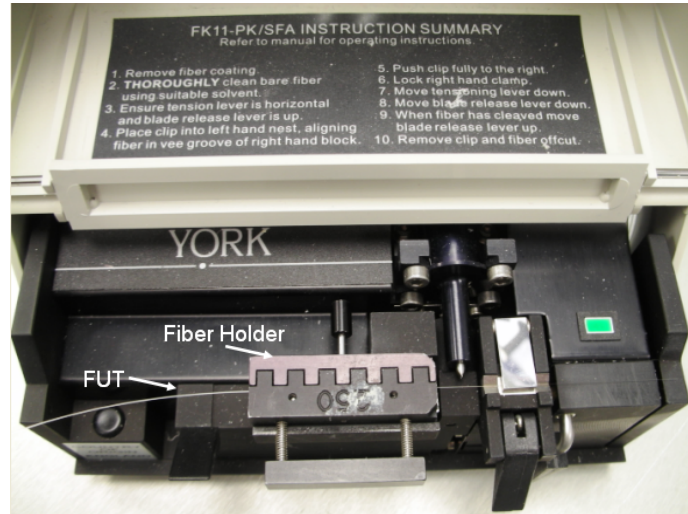


FIGURE 4.8. Fiber holder inserted in cleaver FK 11

For OFL, after 4-5 cm of the buffer coating was stripped off at the input or output ends, the fiber end was cleaned using an alcohol-soaked swab. Then the end was inserted into a fiber holder. After the fiber end was cleaved using a YORK precision fiber optic cleaver FK11 as shown in Figure 4.8, the fiber holder was placed on the input or the output stage of the PK bench. Various diameter mandrels ($r = 2.5$ mm, 5.0 mm, 7.5 mm, and 10.0 mm) with different numbers of turns (1, 2, 5 and 10) were used to induce different amounts of macrobending on the FUT. The power output of the fiber with and without the mandrel wraps was collected, and the bend loss was calculated as:

$$BL(\lambda) = 10 \cdot \log_{10} \left[\frac{P_R(\lambda)}{P_B(\lambda)} \right] \quad (4.2)$$

where $BL(\lambda)$ is the macrobend loss at wavelength λ , $P_R(\lambda)$ is the spectral power measured through the fiber without mandrel wraps, and $P_B(\lambda)$ is the spectral power measured through the fiber with mandrel wraps.

For EFL, the setup and procedure was similar to OFL, but as described in §4.2,

the light power was launched through a two meter length of standard OM3 MMF with 1 turn at 25 mm bend diameter. The output end of the standard OM3 MMF was buffer stripped and cleaned following the same stripping and cleaning procedures as described above for OFL, then it was cleaved using a SIECOR cleaver as shown in Figure 4.9; the input end of the FUT was also processed the same way as the output end of the standard OM3 MMF.



FIGURE 4.9. Fiber inserted in a SIECOR cleaver

Then the standard OM3 MMF and FUT were spliced together using an Ericsson Fusion Splicer shown in Figure 4.10.



FIGURE 4.10. Ericsson fusion splicer

The simplified macrobend loss measurement setup with OFL is illustrated in Figure 4.11, with EFL is presented in Figure 4.12.

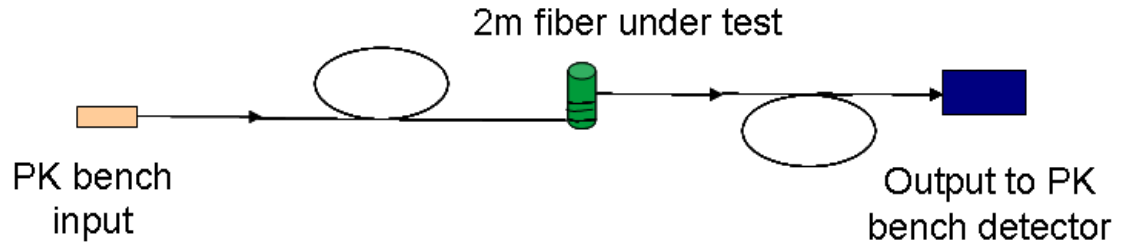


FIGURE 4.11. Macrobend loss measurement setup with an OFL

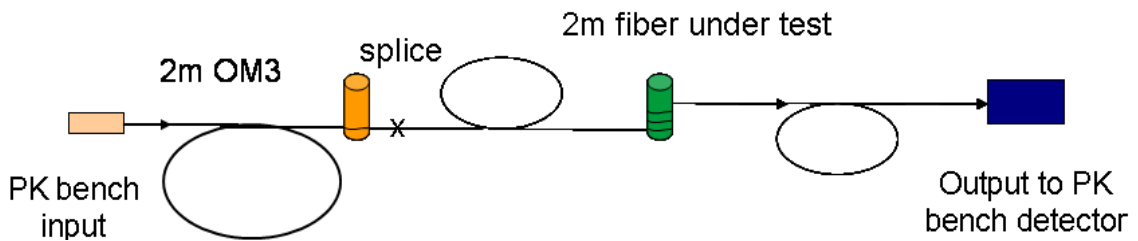


FIGURE 4.12. Macrobend loss measurement setup with an EFL

4.3.2 Results and Findings

First, two standard MMFs described in §3.3, standard MMF1 and standard MMF2, were characterized under each macrobending condition. The spectral scans of the fibers are slightly up-trending curves with an oscillation pattern as shown in Figure 4.13, which shows the result for a standard MMF2 OFL bend loss measurement with 1 turn at 7.5 mm bend radius. The oscillation pattern was explained in [1] as cutoff bumps of the MGs. The n_{eff} of the MG p decreases when the wavelength increases, causing an increased attenuation. When the condition of $n_{eff}(p) = n_{cl}$ is met, that MG p is completely cutoff. The next MG $p - 1$ has a higher $n_{eff}(p - 1)$, so the bend

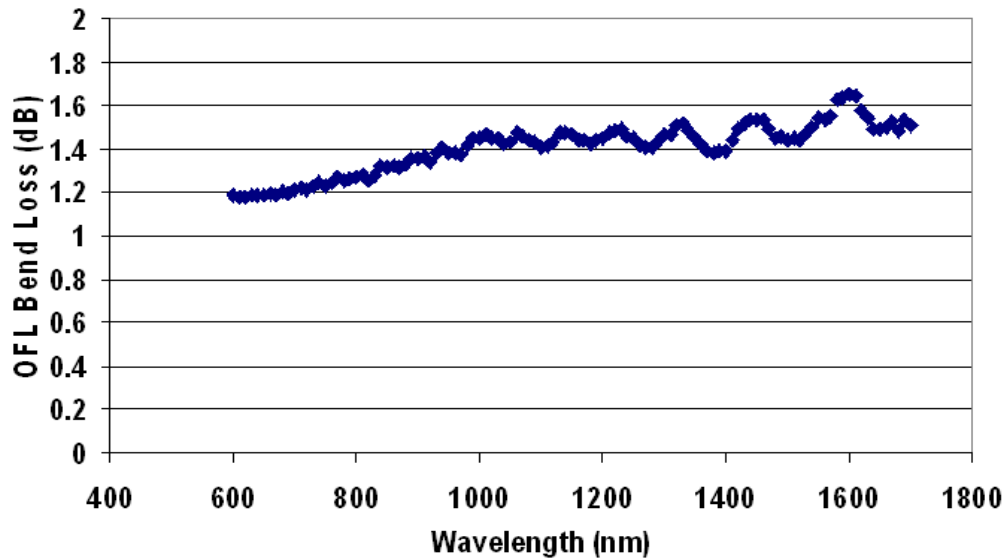


FIGURE 4.13. Spectral scan of standard MMF2 OFL bend loss measurement with 1 turn at 7.5 mm bend radius

loss goes lower first, then it goes up again as the attenuation increases along with the wavelength.

In Figure 4.14, the X axis presents the number of turns at a certain bend radius, and the Y axis is the measured bend loss induced by wrapping the fiber around the mandrel with an OFL. As expected, when the bend radius decreases and the number of turns increases, the amount of light that leaks out of the core increases. Outer (higher order) MGs are more sensitive to bending as reported in [1]. At each bend radius the bend loss increases quickly for the first few turns, then flattens out for larger numbers of turns as the outer MGs are stripped out and inner (lower order) MGs are insensitive to the bending. From the DMD plots presented in Figure 3.5 and Figure 3.6, although the spread of MG delays in standard MMF1 DMD is much broader than in standard MMF2, both fibers' highest order MGs radial positions are very close to the 25 μm core edge and the power distribution of different MGs is also very similar for both fibers. Therefore, standard MMF1 in Figure 4.14 (a) and

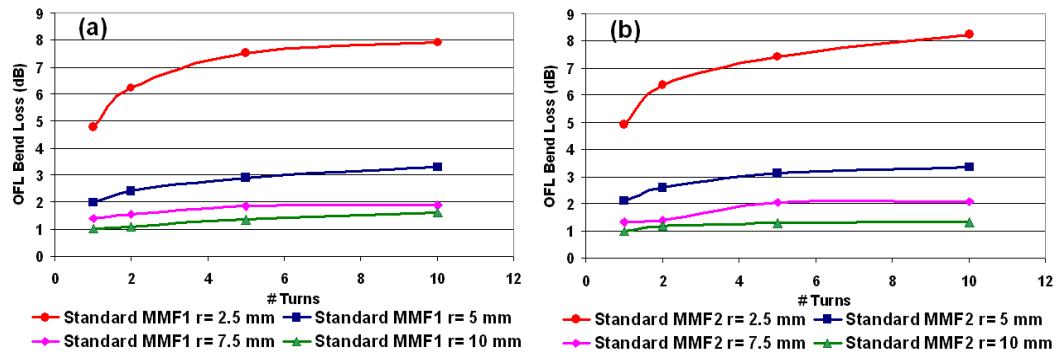


FIGURE 4.14. Measured OFL bend loss at 850 nm with different number of turns at different bend radii. (a) standard MMF1, (b) standard MMF2

MMF2 in Figure 4.14 (b) have similar bend loss behaviors even though they have very different bandwidth (see Chapter 5 for definition) performance.

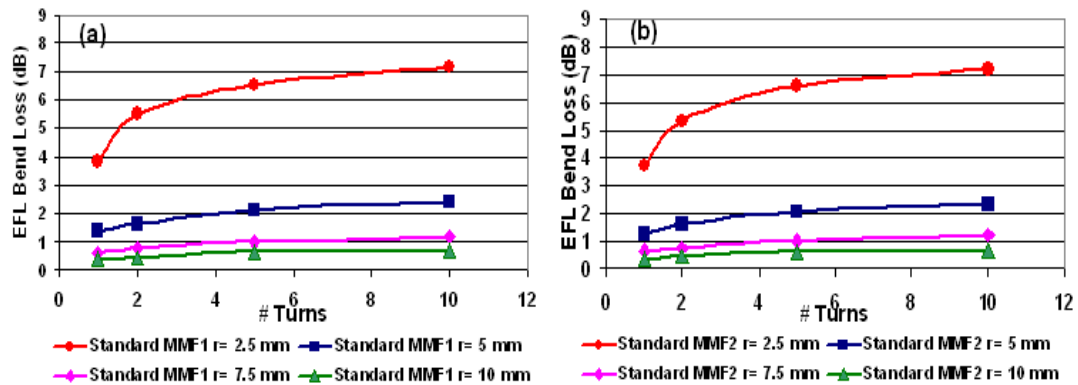


FIGURE 4.15. Measured EFL bend loss at 850 nm with different number of turns at different bend radii. (a) standard MMF1, (b) standard MMF2

With EFL, as shown in Figure 4.15, at different bend radii, the macrobend losses of both standard MMF1 and standard MMF2 also exhibit a similar natural log dependence on the number of turns as with OFL. Under the same bending condition, the bend loss is much lower with EFL than with OFL (Figure 4.14). Outer MGs are more sensitive to bending, and as discussed in §4.2, the relative normalized MG

power shifts from outer radius to inner radius with EFL. With a significant relative power shift from the outer MGs compared to OFL, when those MGs are stripped out by induced macrobending, it has less impact on the transmitted power, and power attenuation is also reduced .

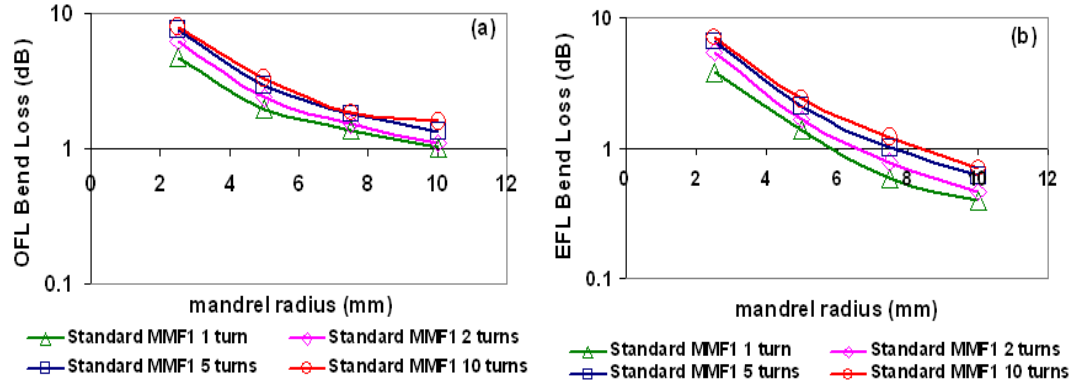


FIGURE 4.16. Comparison of standard MMF1 bend loss performance with (a) OFL and (b) EFL

Figure 4.16 gives another perspective to evaluate the impact of different launch conditions on the fiber bend loss performance. Standard MMF1 bend losses under OFL and EFL are compared directly. The Y axis is the measured bend loss on a log scale, which has an inverse exponential relationship to the bend radius. At a relative large bend radius such as 10 mm, only a few MGs at the very outside core will be impacted by macrobending. Under different launch conditions, those MGs also have a substantial power distribution difference as shown in Figure 4.5, resulting in a much lower bend loss for standard MMF1 with EFL compared to OFL at 10 mm bend radius. Under different numbers of turns at this bend radius, the bend losses are also more diverged with EFL than with OFL. As the bend radius gets smaller, more MGs are attenuated, and the differences between EFL and OFL power distribution shown in Figure 4.5 become smaller. At bend radius 2.5 mm, the difference in bend loss between OFL and EFL is minute.

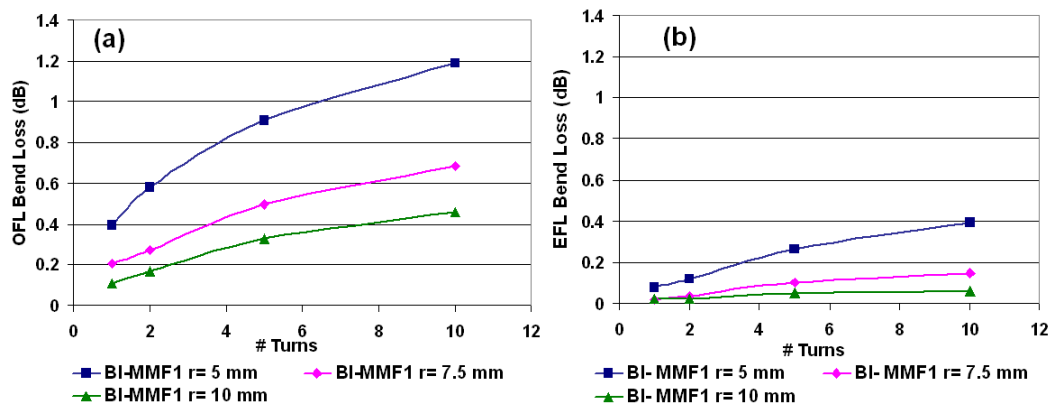


FIGURE 4.17. Measured bend loss of bend optimized MMF at 850 nm (a) OFL, (b) EFL

A new OM2 and OM3 compliant bend-optimized (BO) MMF was recently introduced by Corning Incorporated. This new product was also evaluated and compared to standard MMFs. The bend loss performance shown in Figure 4.17 illustrates that BO MMF are much less sensitive to bending, especially with EFL in Figure 4.17(b).

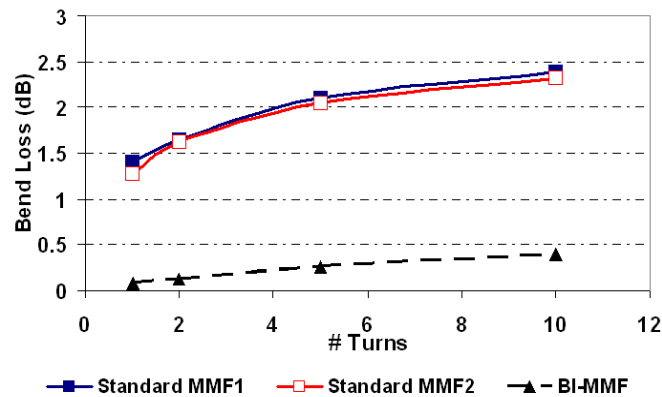


FIGURE 4.18. Bend loss of standard MMF1, standard MMF2, and BO MMF at 850 nm with an EFL using a 5 mm radius mandrel

A comparison of macrobending performance of BO MMF with standard MMFs is shown in Figure 4.18. BO MMF demonstrates exceptional bend resistance even after

ten turns at 5 mm radius.

Chapter 5

IMPACT OF MACROBEND LOSS ON BANDWIDTH

5.1 Bandwidth

As described in Chapter 3, dispersion can be observed as the broadening of pulses in the time domain, but it can also be expressed in frequency domain. For MMFs, Personick [29] has shown that the relationships can be described as :

$$P_{out}(t) = \int_{-\infty}^{\infty} P_{in}(t - \tau)h(\tau)d\tau \quad (5.1)$$

where $h(\tau)$ is the impulse response, $P_{in}(t)$ is the modulating input pulse power, and $P_{out}(t)$ is the detected output pulse.

And

$$F_{out}(f) = F_{in}(f)H(f) \quad (5.2)$$

where $H(f)$ is the system transfer function, $F_{in}(f)$ is the spectrum of the input pulse, or the Fourier transform of $P_{in}(t)$:

$$F_{in}(f) = \int_{-\infty}^{\infty} P_{in}(t)e^{-2\pi ift} dt \quad (5.3)$$

and $F_{out}(f)$ is the spectrum of the output pulse, can be calculated as the Fourier transform of $P_{out}(t)$:

$$F_{out}(f) = \int_{-\infty}^{\infty} P_{out}(t)e^{-2\pi ift} dt \quad (5.4)$$

MMFs are often characterized by their bandwidth [30], which is defined as the baseband frequency f at which the transfer function $|H(f)| = 0.5$. Or in a log scale, $10 \cdot \lg(|H(f)|) = -3dB$ as show in Figure 5.1:

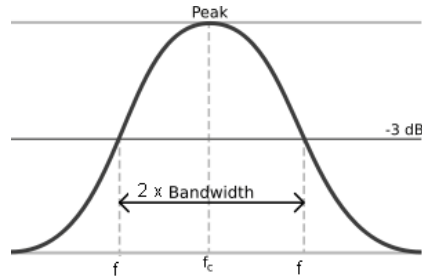


FIGURE 5.1. Transfer function

The advantage of MMF bandwidth characterization is this approach can decouple the light source power variation from the MMF performances in the intermodal dispersion evaluation. The transfer function $H(f)$ can be obtained as the ratio of the Fourier transforms of the output and input pulses as:

$$H(f) = \frac{F_{out}(f)}{F_{in}(f)} \quad (5.5)$$

5.2 DMD Traces Change with Macrobending

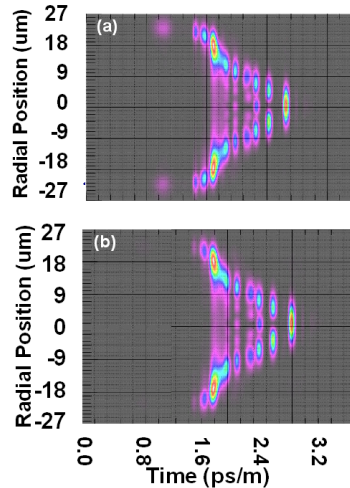


FIGURE 5.2. DMD measurement of standard MMF1 at 850nm. (a) no mandrel bend (b) 1 turn at 5 mm radius

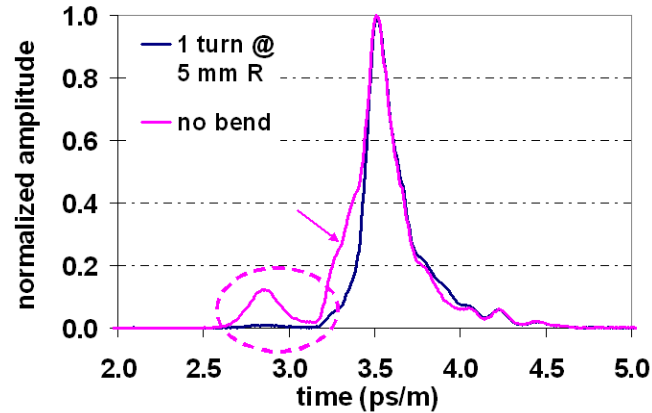


FIGURE 5.3. Pulse measurement of standard MMF1 at 850nm.

Now take a look at DMD of standard MMF1 again in Figure 5.2. Compared to Figure 5.2 (a) where there is no mandrel wrap of the fiber, Figure 5.2 (b) shows that after 1 turn at 5 mm radius, several outer MGs at $R \approx 22 \mu\text{m}$ were completely stripped out, and others were partially attenuated due to the induced macrobending. The inner MGs are well-confined in the core and are not impacted by this bend condition. By stripping some outer MGs, the spread of mode group delays in the DMD is compressed, which should lead to an improvement in the bandwidth.

This result is consistent with the disappearing of the leading shoulder in the amplitude versus time trace shown in Figure 5.3. One turn at 5 mm radius removes some power from outer modes as can be seen in Figure 5.3 (circled area), and improves the pulse shape (area pointed at by the arrow), which should lead to an increase of the bandwidth of the fiber.

On the other hand, the DMD trace for standard MMF2 has very low relative delays between the majority mode groups as shown in Figure 5.4. Stripping out some outer MGs has limited impact on the mode groups delay. Standard MMF2 pulse shape in the time domain (Figure 5.5) shows that although the leading shoulder of the pulse is diminished by induced macrobend, both pulse shape and pulse width are

almost the same as without the macrobend. Therefore, the fiber bandwidth will not be very different with or without macrobending.

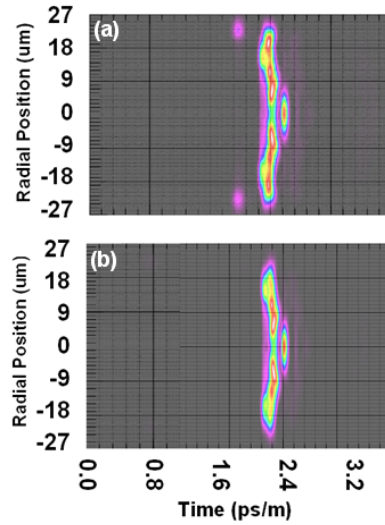


FIGURE 5.4. DMD measurement of standard MMF2 at 850nm. (a) no mandrel bend (b)1 turn at 5 mm radius

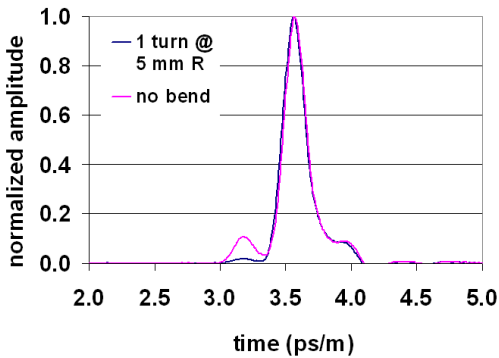


FIGURE 5.5. Pulse measurement of standard MMF1 at 850nm.

The DMD trace of the recently developed BO-MMF introduced in Chapter 4, as presented in Figure 5.6, shows an even more confined spread of mode group delays. The time scale here is about 3 times compressed than the time scales in Figure 5.2

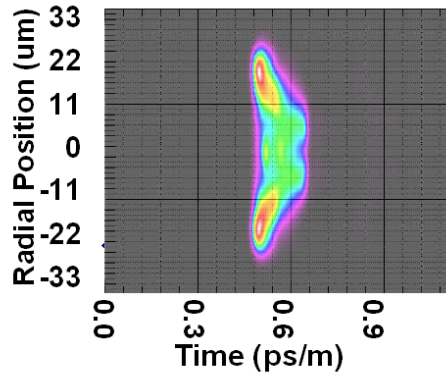


FIGURE 5.6. DMD measurement result of BO-MMF

and in Figure 5.4. The power distribution is also more uniform across the radius, with less localized “high” or “low” intensity features than standard MMF1 and MMF2. Stripping out some outer MGs of this fiber would not notably impact the bandwidth at all.

5.3 Impact of Macrobend Loss

To validate the findings for the DMDs with macrobend described in §5.2, a series of bandwidth measurements using different macrobending conditions with both OFL and EFL were conducted.

5.3.1 Experimental Setup

The same test bench as used in §4.3, the PK 2500 fiber analysis system (Figure 4.7) was also utilized to measure the fiber bandwidth at 850 nm using a different bench execution macro program. The fiber samples preparation and OFL, EFL setup are very similar to the procedures details in §4.3, and the focus here is on the setup related to the bandwidth measurement. The bandwidth concept described in §5.1 was applied, a pulse was launched from the PK bench 850 nm laser source through a

series of optical elements into the fiber under test. The pulse spreading of ~ 2.2 km length of FUT $P_{out}(t)$ was measured and stored. Two $P_{out}(t)$ measurements results with an OFL of standard MMF1 are shown in Figure 5.7 as examples:

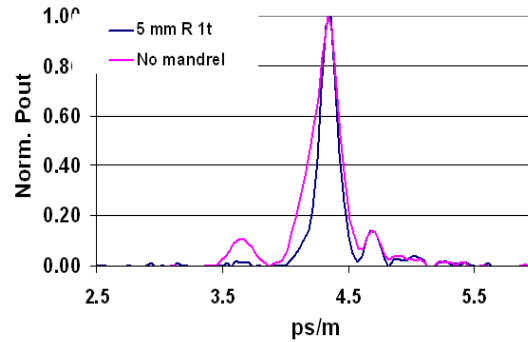


FIGURE 5.7. Examples of measured pulse spreading $P_{out}(t)$ of standard MMF1 with an OFL

where the pulses are normalized by the length of FUT. The pulse in pink is when there is no mandrel wrap of the fiber, the pulse in blue is after 1 turn at 5 mm bend radius.

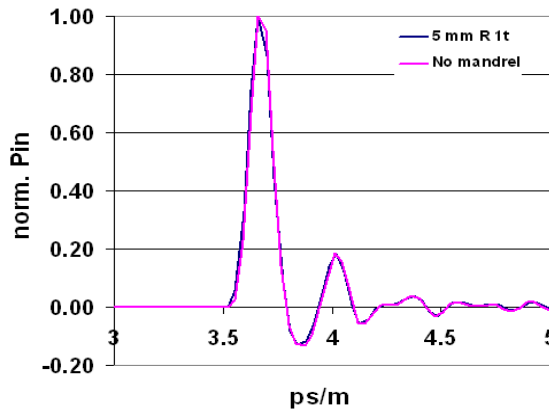


FIGURE 5.8. Examples of measured pulse spreading $P_{in}(t)$ of standard MMF1 with an OFL

Then cutback a 2 m piece of reference fiber was cut from the FUT and measured

the pulse spreading of this reference fiber was measured to determine $P_{in}(t)$. Again, two $P_{in}(t)$ measurements results with an OFL of standard MMF1 are shown in Figure 5.8 as examples, and the pulses are normalized by the length of FUT to be comparable to $P_{out}(t)$ measurements.

The reference was then deconvolved from the output pulse by taking the Fourier Transform of $P_{out}(t)$ and $P_{in}(t)$ and looking at the ratio as expressed in Equation 5.5: $\left| \frac{F_{out}(f)}{F_{in}(f)} \right| = |H(f)|$. The $-3dB$ bandwidth was identified as the frequency f where $10 \cdot \lg(|H(f)|) = -3dB$ as shown in Figure 5.9:

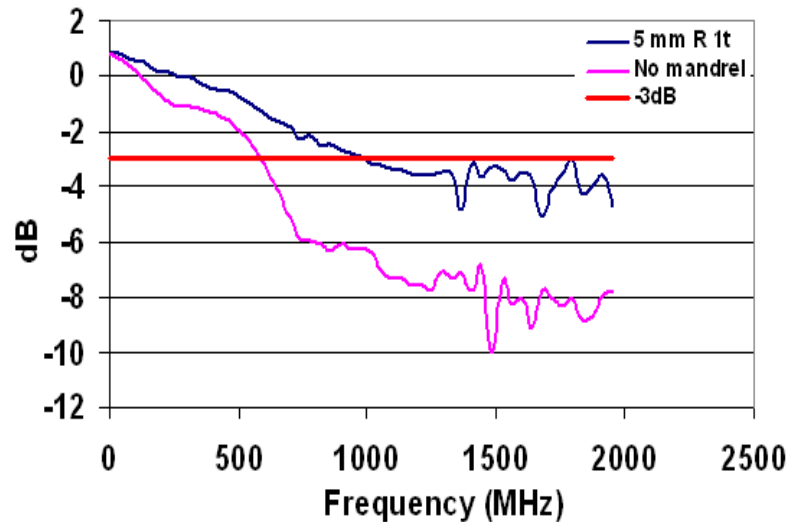


FIGURE 5.9. Examples of bandwidth f identification of standard MMF1 with an OFL

The bandwidth f was then multiplied with the test length of the fiber to calculate the normalized bandwidth which accounts for the pulse broadening increase with the travel distance.

The simplified bandwidth measurement setup with OFL is illustrated in Figure 5.10, the setup with EFL is presented in Figure 5.11.

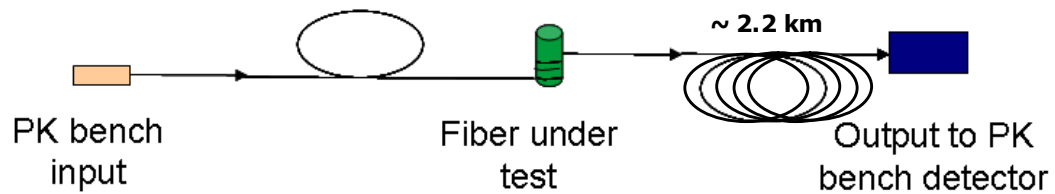


FIGURE 5.10. Bandwidth measurement setup with an OFL

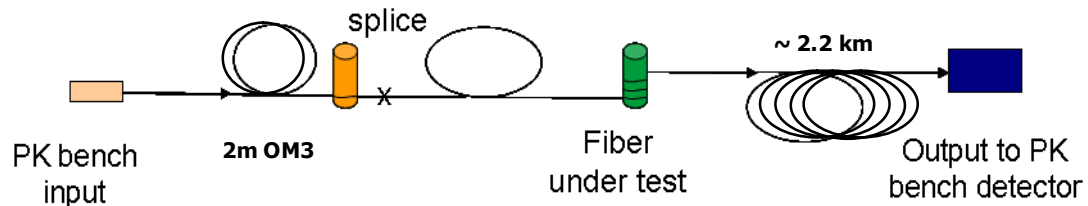


FIGURE 5.11. Bandwidth measurement setup with an EFL

5.3.2 Results and Findings

The same as for bend loss measurements, macrobending was induced by using mandrels of different radii ($r = 5$ mm, 7.5 mm, and 10 mm) with a different number of turns (1, 2, 5 and 10). The three fibers tested in §4.3 were tested again for bandwidth. Without any induced macrobending and with an EFL, standard MMF1 bandwidth is 1830 MHz · km; MMF2 has a bandwidth of 3090 MHz · km; and BO-MMF has a bandwidth of 3500 MHz · km. Those bandwidth results are consistent with their respective fibers' DMD performances.

For standard MMF1 and MMF2, the results are summarized in Figure 5.12. There is a trade-off between the bend loss and the bandwidth for MMF1 with both OFL and EFL, which is expected based on the discussion in §5.2, and the fiber is less sensitive to macrobend under EFL. For standard MMF2, the bandwidth remains high under different bending setups, but similar to standard MMF1 the bend loss increases by as

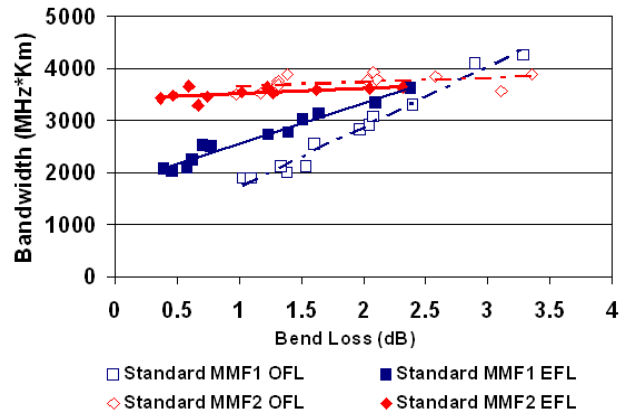


FIGURE 5.12. Impact of macrobend loss on bandwidth with OFL and EFL for standard MMFs

much as 2.5 dB with EFL, or 3.5dB with OFL when the mandrel radius is reduced or the fiber bend length is increased.

Compared to standard MMFs, the new bend-optimized MMF is immune to the deployment condition as presented in Figure 5.13. The fiber is able to maintain high bandwidth and high bend loss resistance consistently.

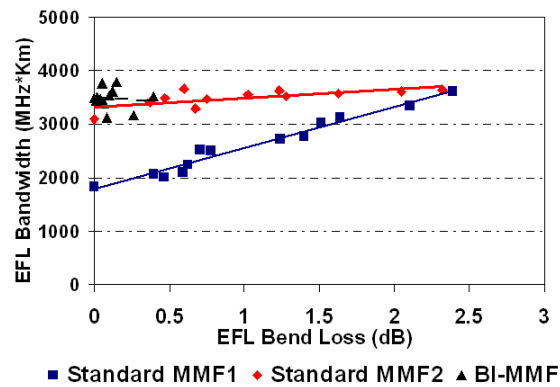


FIGURE 5.13. Impact of macrobending on bandwidth of bend optimized MMF, compared to standard MMFs.

Chapter 6

IMPACT OF MACROBENDING ON OPTICAL LINK PERFORMANCE

As discussed in §3.2 on attenuation and dispersion, particularly in MMF, the modal dispersion can deteriorate signal quality severely and cause data bit errors. In the previous Chapters the impact of macrobending on bend loss and bandwidth were also investigated. In some cases, there are trade-offs between the two. Will it be possible to improve the bandwidth by introducing macrobends to the fiber cable and thus improve overall fiber link performance? In this Chapter, the IEEE link model is used to evaluate the overall system impact.

6.1 Optical Fiber Data Link

A typical optical fiber data link [31] consists of transmitter, a length of optical fiber, several connectors and a receiver. Transmitters as discussed in §2.2.3 are either LEDs, DFBs, FPs, or VCSELs. Light is coupled into the optical fiber, typically 50/125 μm or 62.5/125 μm for MMFs. There are different types of connectors, SC and ST connectors are the most common (in Figure 6.1).

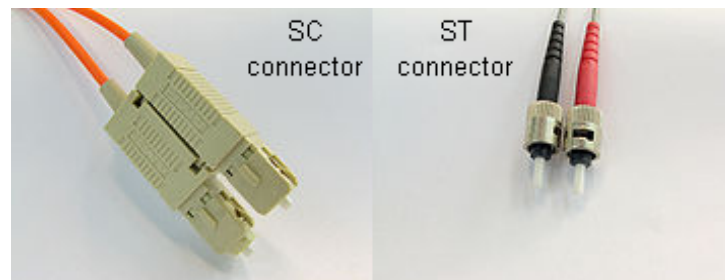


FIGURE 6.1. SC and ST connectors

After the light propagates through the fiber it is collected by the receiver, a PIN or avalanche photodiode. A diagram of a typical data link with MMF [32] is shown in Figure 6.2

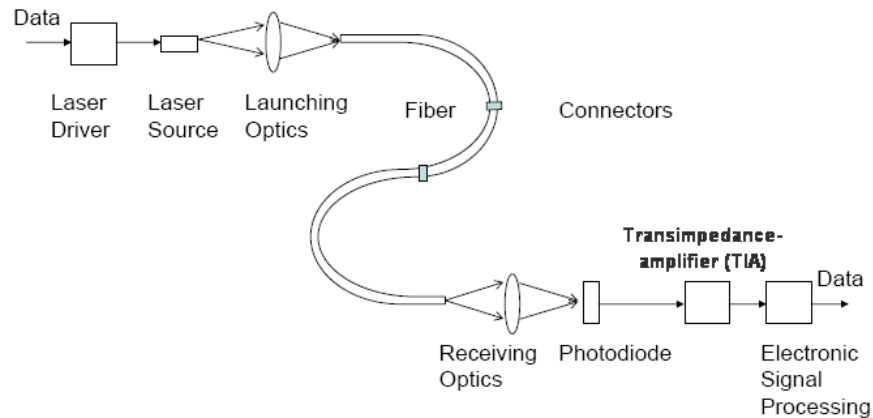


FIGURE 6.2. Typical optical fiber link diagram

Each component in the link has its own limitations, and it will typically not be able to function at its best performance when integrated with the other components in the link. Therefore, a link model is necessary to evaluate the overall optical link performance considering the parameters and limitations of all the components. IEEE GbE and 10 GbE system link models were also developed along with the IEEE GbE and 10 GbE standards.

6.2 10 Gigabit Ethernet Link Model

The link model is a power budget model based on the power conservation equation [33] [34].

$$Power_{out} = Power_{in} - Losses - linkmargin \quad (6.1)$$

where $Power_{in}$ is the optical power launched into the fiber by the transmitter. $Power_{out}$ is the power delivered to the receiver, and there are two types of the losses: power

loss and power penalty. Power loss can be measured with an optical power meter and accounts for connector loss and fiber attenuation. Power penalty can be determined from an eye diagram, and is allocated for system impairments such as noise and dispersion. Power penalties can be calculated to account for:

- inter-symbol interference (P_{ISI}), which is caused by modal dispersion;
- finite laser extinction ratio (P_{ϵ}), which occurs when a non-zero power level is transmitted for a "zero";
- relative intensity noise (P_{RIN}), which is a noise term due to the fluctuation in the output intensity of the laser;
- mode partition noise (P_{MPN}), which is also due to modal dispersion, different laser modes travel with different velocity in a dispersive fiber;
- receiver eye opening (P_{eye}), which accounts for the required finite eye opening width needed by the clock and data recovery.

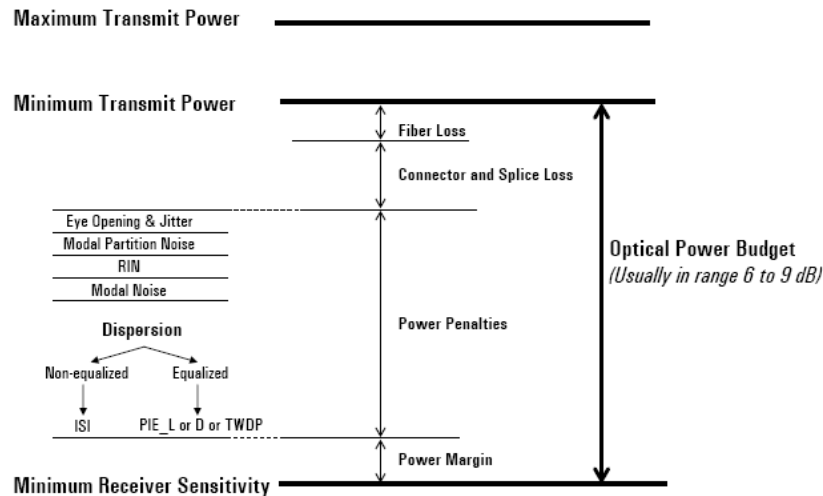


FIGURE 6.3. Optical link power budget

The link margin is the safety margin of power. David Cunningham created a good illustration of the power conservation equation 6.1 in [32] as shown in Figure 6.3, which helps to understand the relationship of those defined terms above.

The IEEE 10 GbE link model (10GEPBud3_1_16a.xls) used for the development of 10 GbE is available at the IEEE P802.ae 10Gb/s Ethernet Task Force website. It is an extensive excel spreadsheet work-book, and each tab is dedicated to a different kind of fiber. The model is viewed to perform a reasonable worst case power budget analysis. It contains some assumptions, for example that a) transmitters have a Gaussian impulse response with a similar step response for rising and falling edges, b) fibers have a Gaussian impulse response, c) receivers have a non-equalized, raised-cosine response, and d) modal noise introduced by partial optical mode coupling in the cable plant is limited to a noise penalty, P_{MPN} , of 0.3dB by limiting the maximum connector loss to 1.5dB.

In this study, the link model spreadsheet assigned for 50 $\mu\text{m}/125 \mu\text{m}$ MMF at 850 nm was used. The industry standard values from the spreadsheet were adopted for transmitter and receiver parameter inputs. For fiber input parameters, some alternative values for attenuation and dispersion were used instead of the default values.

The measured fiber bandwidth under different deployment conditions was input as the modal bandwidth of the respective link. Those fiber input parameters are indicated by the blue frame on a portion of a link model shown in Figure 6.4. Inside the green frame are some system link parameters. The link length this study is interested in is 0.3 km. The power budget also takes a spreadsheet default value of 7.3 dB. When there is no bend, C is at the maximum connector loss limit of 1.5 dB. When macrobend is induced the bend loss is added to the parameter C. Therefore, the difference between power budget P and modified connection loss C (P-C) is the allowable limit for the sum of fiber attenuation and any other power penalties. The link margin is the difference between P-C and the attenuation plus the power penalties. The link margin and power penalties outputs under different macrobend conditions and launch conditions are the focus of this study. Link margin is marked within the red frame. The outputs inside the pink frame are the calculated

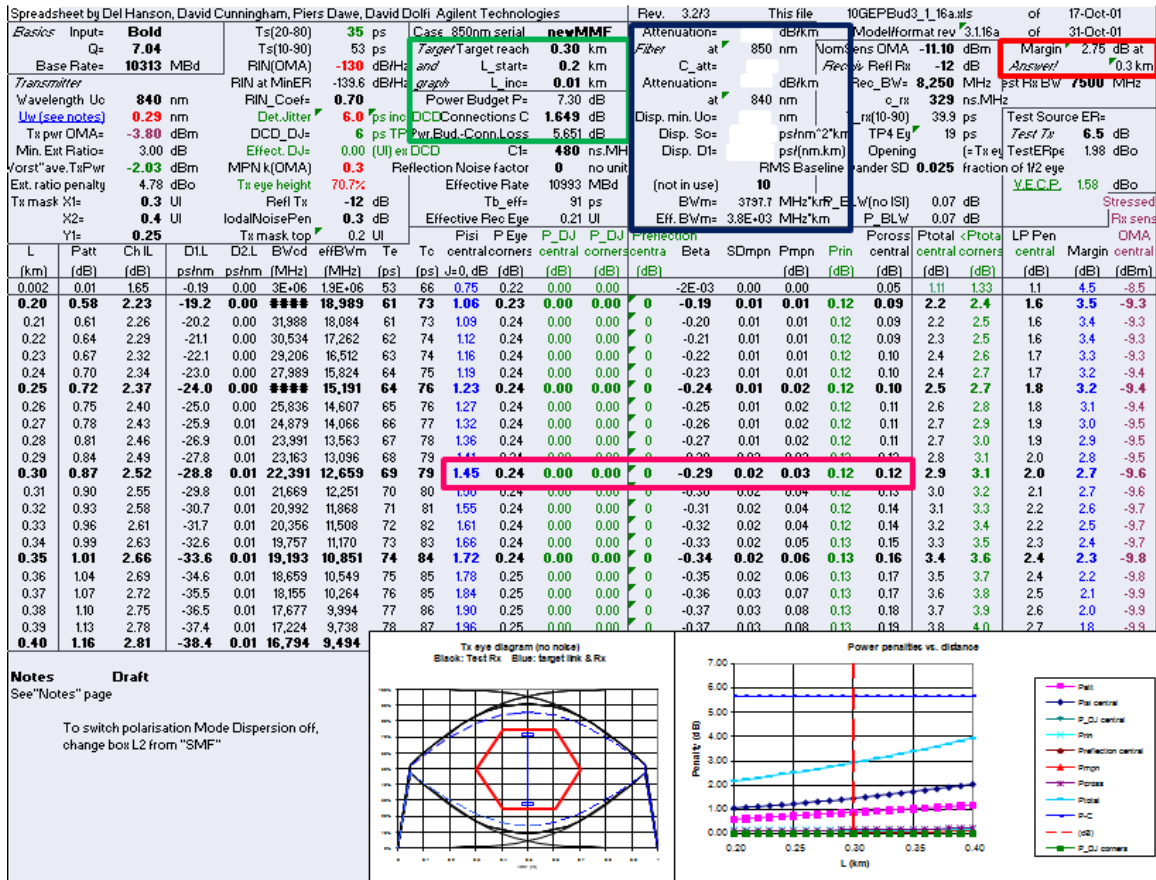


FIGURE 6.4. Portion of the IEEE 10GEPBud3_1_16a.xls spreadsheet

power penalties. The P_{ISI} is particularly important because in the presence of inter-symbol interference (ISI), each 0-1 transition is different from any other and likewise with the 1-0 transitions. The ISI manifests itself in the eye diagram as horizontal and vertical closures of the eye as shown in Figure 6.5. Therefore, the IEEE 10 GbE standard committee is very conservative about P_{ISI} and set 3.6 dB as the acceptable limit.

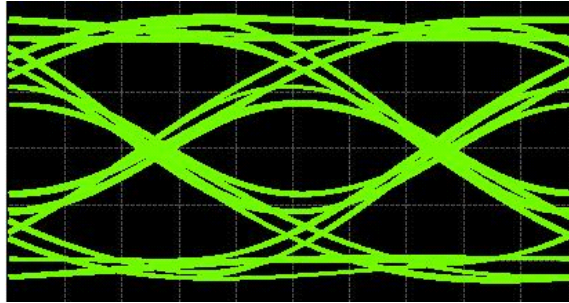


FIGURE 6.5. An eye diagram shows the presence of ISI

6.3 Results and Findings

First, consider a few examples of the modeling outputs in power penalties vs. link length and Tx eye diagrams. The P-C limit is driven by bend loss. A higher bend loss will cause a lower acceptable P-C value. The total power loss P_{total} , or the sum of fiber attenuation and any other power penalties, increases with the link length. The main contributors to P_{total} are fiber attenuation and P_{ISI} . Since the same attenuation coefficient is applied to all the samples, the attenuation for different samples is the same at 0.3 km. Therefore, P-C limit and P_{ISI} are the main variables of the link performance under different deployment conditions.

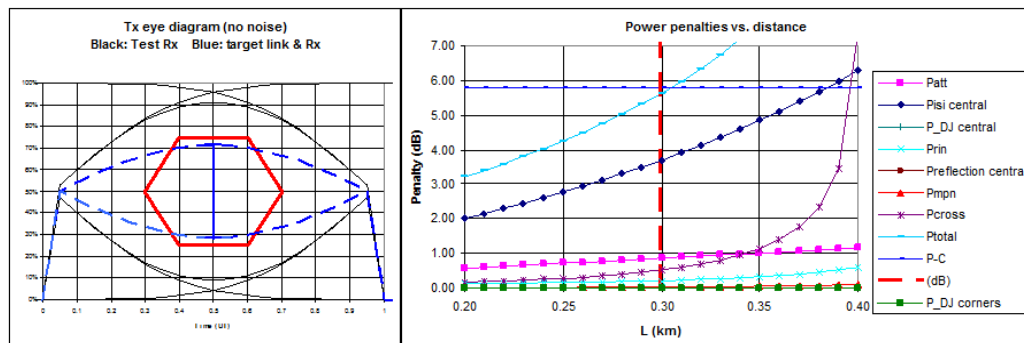


FIGURE 6.6. Standard MMF1 with no bend, with an OFL

The results for standard MMF1 with no bend and with an OFL in Figure 6.6

shows that this link suffers from high P_{ISI} . The eye is closed within the eye mask boundary in red, and even though there is some link margin available the link will not work.

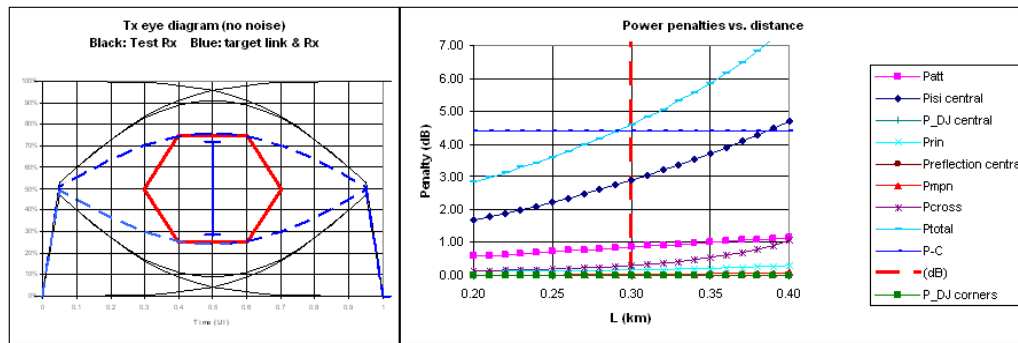


FIGURE 6.7. Standard MMF1 with 1 turn at 7.5 mm bend radius, with an OFL

After 1 turn at 7.5 mm bend radius, the modal bandwidth is improved as already discussed in §5.3.2., however the P-C value also drops along with increasing bend loss. For this link, as shown in Figure 6.7, the improved P_{ISI} leads to an eye diagram that is slightly opened up and closer to the edge of the eye mask, and the total power loss is also slightly above the P-C limit.

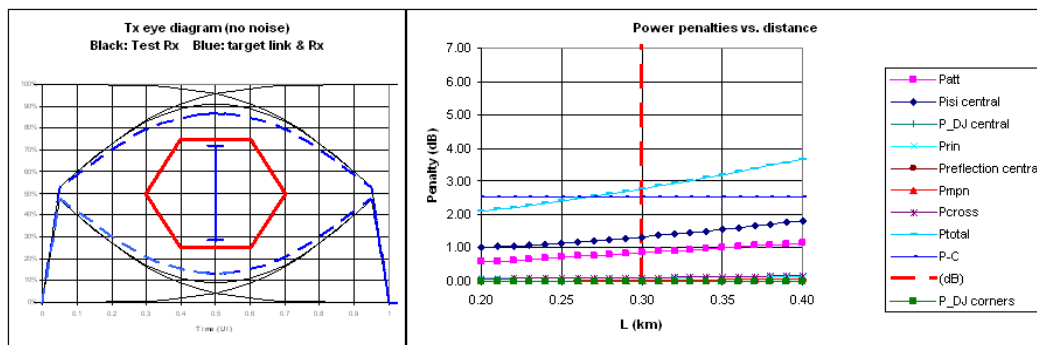


FIGURE 6.8. Standard MMF1 with 10 turn at 5 mm bend radius, with an OFL

After 10 turns at 5 mm bend radius, as shown in Figure 6.8, the eye is wide open, but the induced bend loss is so high that the P-C limit is below the total power loss,

and the link fails.

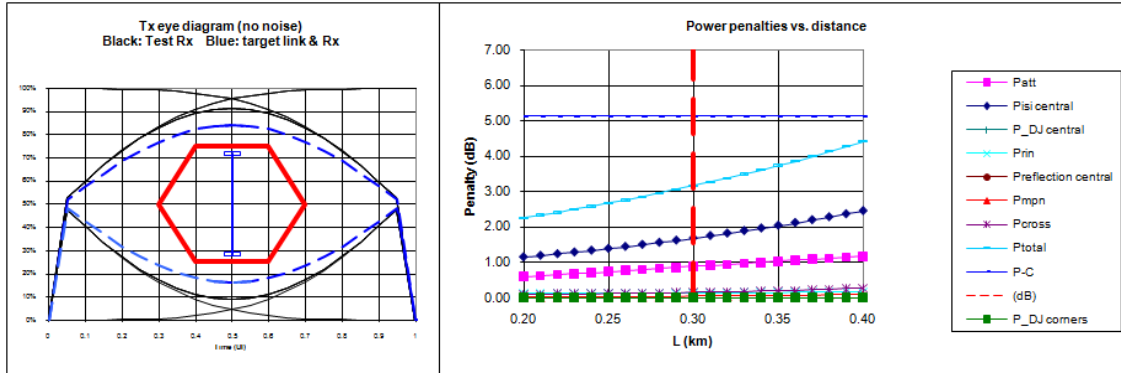


FIGURE 6.9. BO- MMF with 10 turn at 7.5 mm bend radius, with an OFL

As shown in Figure 6.9, for BO-MMF with 10 turns at 7.5 mm bend radius with an OFL the bend loss is so low that there is enough margin for the P-C limit, and the overall link margin is 1.96 dB. In addition, the eye diagram is also wide open with a good ISI performance. The model predicts that this link will work well.

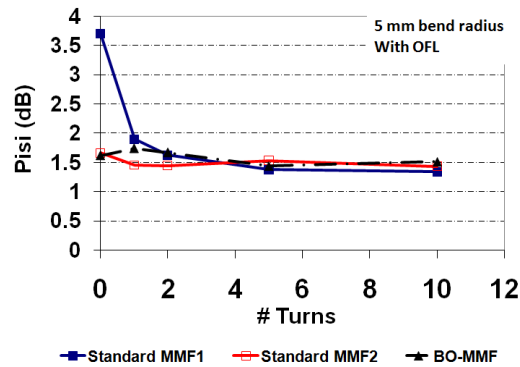


FIGURE 6.10. P_{ISI} at 5 mm bend radius with OFL

From Figure 6.10 and Figure 6.11, for standard MMF1 with a low bandwidth performance when there is no bend, P_{ISI} of the link is high with both OFL and EFL. Especially with OFL it is above the 3.6 dB limit. After the macrobending is induced

on the fiber, the P_{ISI} performance is improved. Both standard MMF2 and BO-MMF have good bandwidths, so the optical links of those fibers have low and consistent P_{ISI} values under different deployment conditions.

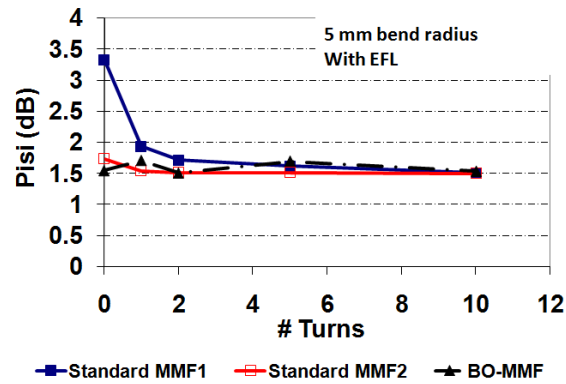


FIGURE 6.11. P_{ISI} at 5 mm bend radius with EFL

The summarized modeling results of link margin at 5 mm bend radius with OFL are shown in Figure 6.12. The links using standard MMF1 will not work at all. For standard MMF2, once the macrobending is induced, the link performance starts to drop, and after 1 turn, the modeled link fails. For BO-MMF, the link works at all different bending conditions.

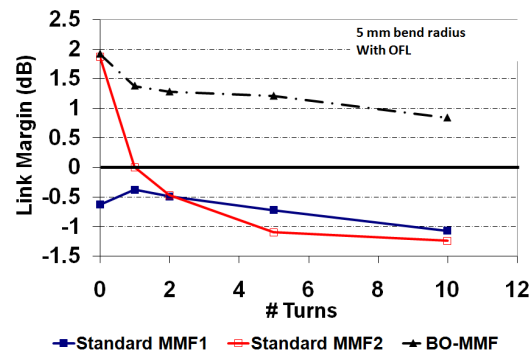


FIGURE 6.12. Link margin at 5 mm bend radius with OFL

The observation is very similar with EFL as shown in Figure 6.13. There are some improvements on the link performance for standard MMFs. With a small number of turns, the link margin of standard MMF1 increases slightly because the bandwidth is enhanced by induced macrobending. As the number of fiber turns increases, the impact of higher bend loss surpasses the bandwidth improvement, and the modeled link fails. Based on the modeling, the link margin of standard MMF2 also drops below the acceptable level after 5 turns of the fiber. On the other hand, BO-MMF is able to maintain a high link margin under all conditions.

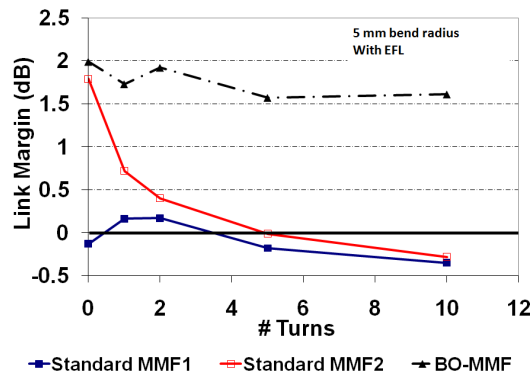


FIGURE 6.13. Link margin at 5 mm bend radius with EFL

Overall, both bend loss and bandwidth of the fiber are important to the optical link performance. Compared to standard MMFs, BO-MMF is more robust under different deployment conditions.

Chapter 7

CONCLUSIONS AND FUTURE WORK

7.1 Conclusions

The objectives of this study are: a) to investigate the impact of both OFL and EFL conditions on MMF performance, b) to understand the impact of macrobending on MMFs bend loss, bandwidth, and the overall 10 GbE link performance, and c) to investigate desired MMF parameters for an optimal 10 GbE link. Series measurements were conducted using a PK 2500 fiber analyzer and a fiber DMD bench at 850 nm to evaluate the impact of macrobend loss on bandwidth of selected MMFs under not only OFL condition but also EFL, which is a more relevant launch condition to the VCSEL transmission. The macrobending was induced by using mandrels of different diameters ($r=5$ mm, 7.5 mm, and 10 mm) with different numbers of turns (x1, x2, x5, and x10). For standard MMF1, which has a low bandwidth performance due to the DMD spreading among different MGs, there is a trade-off between the bend loss and the bandwidth. For standard MMF2, which has a high bandwidth, the bandwidth remains high under different bending setups, but similar to standard MMF1, the bend loss increases by as much as 2 dB with an EFL when the mandrel diameter is reduced or the fiber bend length is increased. On the other hand, the BO-MMF is not only insensitive to macrobending, but also able to maintain the high bandwidth at the same time. The overall optical link performance of the selected fibers under all the different deployment conditions was evaluated using the IEEE 10 GbE link model. Improvements of the MMFs performance are observed under the encircled flux launch condition. Both bend loss and bandwidth are critical to 10 GbE link performance. The optical link performance of the standard fiber deteriorates with macrobends. Even using the standard MMF with very high bandwidth, the optical link may still

suffer from significant bend loss under certain macrobending conditions. The BO-MMF is more reliable to different deployment conditions compared to standard MMF. This versatility makes it a promising medium for 10GbE applications.

7.2 Future Work

As the demands of Ethernet data rate continue to grow, the bandwidth of MMF is approaching the current frequency limitation at about 2000 MHz for the commercially purchased PK 2500 fiber analyzer. Therefore, the measurement of a standard 2.2 km fiber will be restricted to less than 4400 MHz · km. As the example shown in

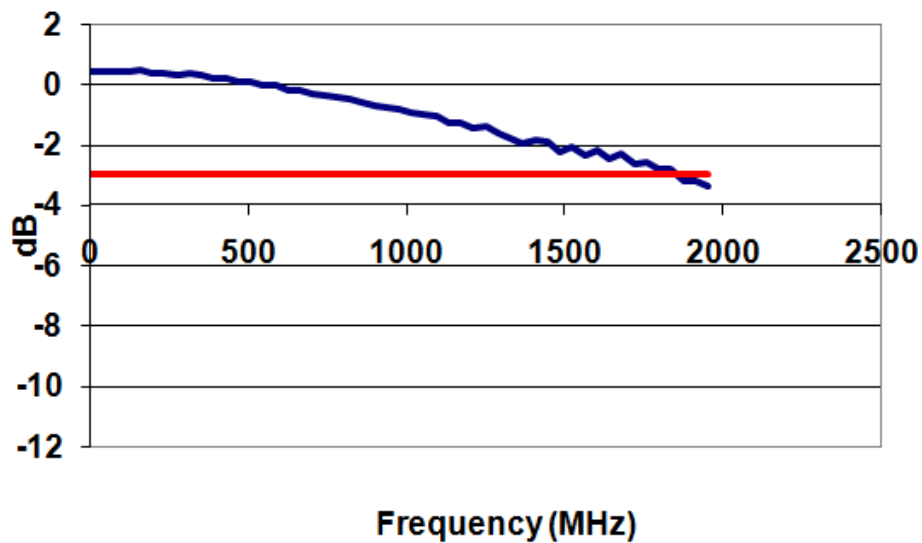


FIGURE 7.1. Example of very high bandwidth measurement result

Figure 7.1, the $10 \cdot \lg(|H(f)|)$ profile of a high bandwidth fiber is flat compared to the profile of standard MMFs shown in Figure 5.9. If the profile is even flatter, the intersection with the -3 dB line will be beyond 2000 MHz, which is above the bench measurement capability. Consequently, emergent higher bandwidth applications are driving necessary measurement system capabilities into new regimes which require

coverage over a much higher frequency range. To validate the hypotheses developed based on those selected signature samples, additional examples need to be included. In this study, the link performance was evaluated using the IEEE link model simulation. The next step is to construct links of different lengths using the selected MMFs and test for BER to validate the IEEE link model results.

REFERENCES

- [1] MOLIN, D., MATTHIJSSE, P., KUYT, G., and SILLARD, P., “Reduced bend sensitivity of multimode fibers in FttX applications,” *Proceedings of the 56th IWCS*, pp. 348–353, 2007.
- [2] Cisco Systems, *Internetworking Technology Handbook*, 2008.
- [3] RADHAKRISHNAN, G., “Next-generation 50um fiber enhances 10 gigabit ethernet performance,” *Corning Incorporated White Paper*, 2002.
- [4] BELL, P., “Fiber selection guide for premises networks,” *Corning Incorporated White Paper*, 2007.
- [5] MARCUSE, D., *Principles of Optical Fiber Measurement*. Academic Press, Inc., 1981.
- [6] KEISER, G., *Optical Fiber Communications*. McGraw-Hill, 3rd ed., 2000.
- [7] PALAIS, J. C., *Fiber Optic Communications*. Prentice-Hall, Inc., 1983.
- [8] HECHT, J., *Understanding Fiber Optics*. Prentice-Hall Inc., 3rd ed., 1999.
- [9] MARCATILI, E., “Objectives of early fibers: Evolution of fiber types,” *Optical Fiber Telecommunications*, 1979.
- [10] HUTCHESON, M. and PONDILLO, P., “Parallel optic interfaces,” *Cabling Business Magazine*, vol. 11, p. R4185, February 2001.
- [11] BUCK, J. A., *Fundamentals of Optical Fibers*. A Wiley-Interscience Publication, 1995.
- [12] SNYDER, A. W., “Weakly guiding optical fibers,” *J. Opt. Soc. Am.*, vol. 70, pp. 405–411, April 1980.
- [13] GLOGE, D., “Weakly guiding fibers,” *Applied Optics*, vol. 10, pp. 2252–2258, October 1971.
- [14] GHATAK, A. and THYAGARAJAN, K., *Introduction to Fiber Optics*. Cambridge University Press, 1998.
- [15] HECHT, J., “Absorption and scattering determine fiber attenuation,” *Laser Focus World*, pp. 111–118, August 2000.
- [16] FERNANDO, X., “Guided propagation along the optical fiber.” Powerpoint Presentation.

- [17] GOLOWICH, S. E., REED, W. A., and RITGER, A. J., “A new modal power distribution measurement for high-speed short-reach optical systems,” *Journal of Lightwave Technology*, vol. 22, pp. 457–468, February 2004.
- [18] LIU, Y., RAHMAN, B., NING, Y. N., and GRATAN, K., “Accurate mode characterization of graded-index multimode fibers for the application of mode-noise analysis,” *Applied Optics*, vol. 34, pp. 1540–1543, March 1995.
- [19] COLEMAN, D. and BELL, P., “Calculated effective modal bandwidth enhances 10 GbE performance reliability for laser-optimized 50/125 μm multimode fiber,” *Corning Incorporated White Paper*.
- [20] HICKS, V. C., “Multimode fiber certification: Light source launch conditions and encircled flux standard,” 2008.
Application note 196.
- [21] TIA/EIA Fiber Optic Test Procedure, *Mode Scrambler Requirements for Overfilled Launching Conditions to Multi-Mode Fibers, (FOTP) 54*, December 2001.
- [22] TIA/EIA, *Launched Power Distribution Measurement Procedure for Graded-Index Multimode Fiber Transmitters*, June 2001.
Fiber Optic Test Procedure (FOTP) 203.
- [23] PONDILLO, P. and HACKERT, M., “Modal dependence of bandwidth,” *Corning Incorporated White Paper*, 2001.
- [24] PONDILLO, P., “Multimode fiber for use with laser sources,” *Corning Incorporated White Paper*, 2001.
- [25] HANSON, T., “Multimode macrobending loss and launching conditions,” *IEC ad hoc working group on macrobending loss test method*, March 2007.
- [26] *Corning InfiniCor 50 μm Optical Fibers Product Information*.
- [27] GLOGE, D., “Bending loss in multimode fibers with graded and ungraded core index,” *Applied Optics*, vol. 11, pp. 2505–2513, November 1972.
- [28] MARCUSE, D., “Influence of curvature on the losses of doubly clad fibers,” *Applied Optics*, vol. 21, pp. 4208–4213, December 1982.
- [29] PERSONICK, S. D., “Baseband linearity and equalization in fiber optic digital communication systems,” *Bell syst. Tech. J.*, vol. 52, p. 1175, 1973.
- [30] MARCUSE, D., *Principles of Optical Fiber Measurements*.
Academic Press, 1981.
- [31] PONDILLO, P., “Optical fiber local area networks: Bandwidth, data rate, and link length- what does it all mean?,” *Corning Incorporated White Paper*, 2001.

- [32] CUNNINGHAM, D., “Multimode fiber data communication,” *OFC/NFOEC 2008*, 2008.
- [33] NOWELL, M. C., CUNNINGHAM, D. G., HANSON, D. C., and KAZOVSKY, L. G., “Evaluation of gb/s laser based fibre LAN links: Review of the gigabit ethernet model,” *Optical and Quantum Electronics*, vol. 32, pp. 169–192, 2000.
- [34] CUNNINGHAM, D. G. and LANE, W. G., *Gigabit Ethernet Networking*. Macmillan Technical Publishing, 1999.